



Deliverable 3.13

Fabrication of MgB_2 Coils – A superconducting generator pole demonstrator

Agreement n.:	308974
Duration	November 2012 – October 2017
Co-ordinator:	DTU Wind

PROPRIETARY RIGHTS STATEMENT

This document contains information, which is proprietary to the "INNWIND.EU" Consortium. Neither this document nor the information contained herein shall be used, duplicated or communicated by any means to any third party, in whole or in parts, except with prior written consent of the "INNWIND.EU" consortium.

The research leading to these results has received funding from the European Community's Seventh Framework Programme FP7-ENERGY-2012-1-2STAGE under grant agreement No. 308974 (INN WIND.EU).

Document information

Document Name:	Fabrication of MgB ₂ Coils – A superconducting generator pole demonstrator
Document Number:	Deliverable D3.13
Author:	Niklas Magnusson, Svein Magne Hellesø, Morten Ellingsen Paulsen, Jan Christian Eliassen and Asger B. Abrahamsen
Document Type	Report
Dissemination level	PU
Review:	xxxxxxxxxxxxxx
Date:	30 June 2016 & 2 November 2016.
WP:	3 Electro-Mechanical conversion
Task:	3.1.3 MgB ₂ coil
Approval:	Approved by Task Leader



PREFACE

To start with the disappointing news: A malfunction in the current leads of the testing facility obstructed test at full load of the coil before the deadline for issuing this report. Therefore, at the end of this report, an action plan is described for how to solve the issue to allow for a full load test of the MgB₂ superconducting generator pole. Up to this crucial point, this report describes the work performed and the results obtained. It is suggested that the remaining work is reported in the final report.

The work has partly been performed in cooperation with the NOWITECH program and the Norwegian University of Science and Technology, particular by the involvement of Master of Science students. Special thanks are therefore given to Jan Christian Eliassen and Morten Ellingsen Paulsen.

Parts of the present report has its origin in and is extracted from previously published work:

Asger B. Abrahamsen, Niklas Magnusson, Bogi B. Jensen, Dong Liu and Henk Polinder
Design of an MgB₂ race track coil for a wind generator pole demonstration
Journal of Physics: Conference Series vol. 507, 032001, 2014 [1].

N. Magnusson, J.C. Eliassen, A.B. Abrahamsen, A. Nysveen, J. Bjerkli, M. Runde and P. King
Design aspects on winding of an MgB₂ superconducting generator coil
Energy Procedia vol. 80, pp. 56-62, 2015 [2].

Jan Christian Eliassen
Winding and Testing of Superconducting Coils
Master of Science Thesis, Norwegian University of Science and Technology, 2015 [3].

Morten Ellingsen Paulsen
Assembly and Testing of Superconducting Field Winding
Master of Science Thesis, Norwegian University of Science and Technology, 2016 [4].

Table of contents

PREFACE	3
Table of contents	4
1 DESIGN OF COIL DEMONSTRATOR	5
1.1 MgB ₂ superconductor	6
1.2 Coil design parameters	7
1.3 Properties of MgB ₂ wire from Columbus Superconductors	8
1.4 Critical current density scaling of MgB ₂ wire	12
2 WINDING METHODOLOGY	18
2.1 Wet-winded double pancake coils	18
2.2 Epoxy insulated coil	18
2.2.1 Innovative step	18
2.2.2 Turn-to-turn voltages appearing under operation	19
2.2.3 Turn-to-turn resistance in a double pancake test coil	21
2.3 Conclusion – winding methodology	22
3 COIL WINDING AND ASSEMBLY	23
3.1 Winding procedure	23
3.2 Assembly of sub-coils	26
3.3 Soldering	30
4 TESTING PROVISIONS	32
4.1 Mechanical support	32
4.2 Cooling - redesign of cryostat for the particular coil	33
4.3 Current leads	35
4.4 Quench protection	36
4.5 Magnetic field safety	37
5 INITIAL TESTING	38
6 CONCLUSIONS	43
7 ACTION PLAN TO COMPLETE A FULL LOAD TEST	44

1 DESIGN OF COIL DEMONSTRATOR

The MgB₂ demonstration coil of the INN WIND.EU project is a down scaled version of a field coil obtained for a 10 MW MgB₂ superconducting wind turbine generator design [5] based on the properties of the an MgB₂ wire from Columbus Superconductors in Genova Italy [6].

The generator was design for the 10 MW INN WIND.EU reference turbine with the main characteristics of a rated rotation speed of 9.65 rpm resulting in a torque of the shaft in the order of 10.6 MNm [7].

Table 1 is showing the main parameters of the generator, which was design along the philosophy of providing a machine which is “light weight and not too expensive”. This was obtained using a quite large amount of MgB₂ wire in the air-cored field winding and an air-cored armature winding based on copper placed at room temperature. The only usage of silicon iron was to enclose the magnetic flux around the armature winding.

The main dimensions of the resulting machine were an outer diameter in the order of 6.0 m and a stack length in the order of 3.1 m. A rather small generator diameter was targeted in order to fit the superconducting generator in front of the turbine blades of the king-pin based nacelle design chosen for the INN WIND.EU reference turbine [8]. The intension with the design was also to investigate how to use MgB₂ wires in a field winding to produce an airgap flux density in the order of 1.5 T, which is considerable higher than what is used in conventional wind turbine generators. Such a high air gap flux density resulted in flux densities in the superconducting coil in the order of 3.0 Tesla as illustrated in figure 1.1.

Table 1. Main parameters of the MgB₂ direct drive generator designed to comply with the properties of the INN WIND.EU 10 MW reference turbine. [1]

R _{Fe out} [m]	2.94	Torque [MNm]	10.6
R _{Armature out} [m]	2.79	Speed [rpm]	9.65
R _{Armature in} [m]	2.73	Poles [2p]	32
R _{Supercond out} [m]	2.69	Frequency [Hz]	2.57
R _{Supercond in} [m]	2.59	B _{air gap} [T]	1.5
L _{generator} [m]	3.1	Arm. loading [A/m]	10 ⁵
R _{End} [m]	0.15	Arm. Fill [%]	50
W _{coil} [mm]	84	Shear stress [kN/m ²]	75
H _{coil} [mm]	80	Efficiency [%]	97.7
L _{SC single pancake} [m]	740.9	J _{coil} [A/mm ²]	70 @ 3 Tesla
L _{SC double pancake} [m]	1481.7	J _{tape} [A/mm ²]	113 @ 3 Tesla
L _{SC Race track coil} [km]	14.82	M _{Cu} [kg]	19415
L _{SC total} [km]	474.2	M _{Fe} [kg]	24998
Tape unit cost [€]	4	(→ 1) M _{active} [kg]	52331
SC cost [k€]	1897	(→ 474) Cost Cu [€]	291234
M _{Superconductor} [kg]	7918.1	Cost Fe [€]	74994
M _{cryostat+cooler} [kg]	TBD	Cost total [k€]	2263 (→ 840)
Cost cryostat	TBD	Cost / cap. [€/kW]	226 (→ 84)

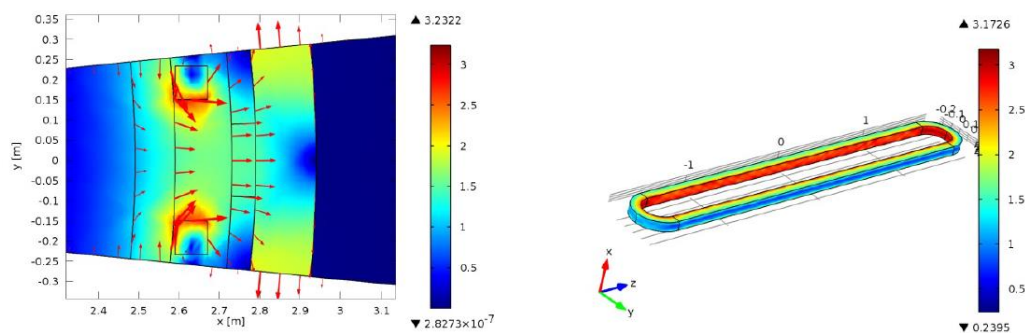


Figure 1.1. Left: Magnetic flux density distribution [Tesla] in cross section of a pole of the 10 MW direct drive generator. Right: Magnetic flux density [Tesla] at surface of MgB₂ race track coil of the 10 MW MgB₂ generator [1].

1.1 MgB₂ superconductor

The choice of using the MgB₂ superconductor for designing the INNWIND.EU generator is based on the fact that MgB₂ was first discovered to be superconducting in 2001 with a critical temperature of $T_c = 39$ K. Due to the simple crystalline structure of the metal alloy MgB₂ it was realized that wires based on filaments in a matrix of nickel could be made by simple drawing techniques. Thus commercial MgB₂ wires with unit lengths of up to 1 km were becoming available at the formulation of the INNWIND.EU project. The advantage of the MgB₂ wires are their relative high critical temperature, which should be compared to the critical temperature of the NbTi wire of the Magneto Resonant Imaging (MRI) industry with $T_c = 9.8$ K and the Nb₃Sn wire being used by the fusion reactor experiment ITER with $T_c = 18$ K.

Secondly the cost of MgB₂ wires is relatively low being in the order of 4 €/m and with a potential to decrease to 1 €/m [6]. This latter is about a factor of 2 higher than for the NbTi wire, but considerable lower than what is seen for the high temperature superconducting tapes of the type RBa₂Cu₃O_{6+x} (R = Rare earth), with unit costs in the range of 20-30 €/m. It should be said that the cost of the high temperature superconducting tapes are expected to reduce as the production volume is scaled up.

Thus MgB₂ is seen as a cost competitive wire with a critical temperature in between the low temperature superconductors (NbTi and Nb₃Sn) and the high temperature superconductors with $T_c = 93$ K.

The properties of the MgB₂ wires used for the 10 MW generator were obtained from the wire manufacture Columbus Superconductors [6]. The most important parameter is the critical engineering current density J_E of the MgB₂ wire, which is defined at the critical current I_c of the wire divided by the wire cross sectional area A_{wire} . Safe operation of a superconducting coil demands that the operation current is sufficiently lower than the critical current. The critical current is however depending the operation temperature as well as the operation magnetic flux density. As the operation current of a superconducting coil is increased then the produced magnetic flux density on the superconductor is also increasing. This is characterized by the load line of the coil and one have to find the operation point by considering that the load line must be sufficiently below the critical engineering current density of a specific temperature. Figure 1.2 is showing the critical engineering current density of the MgB₂ wires operated at different temperatures in comparison to the load line of the 10 MW coil.

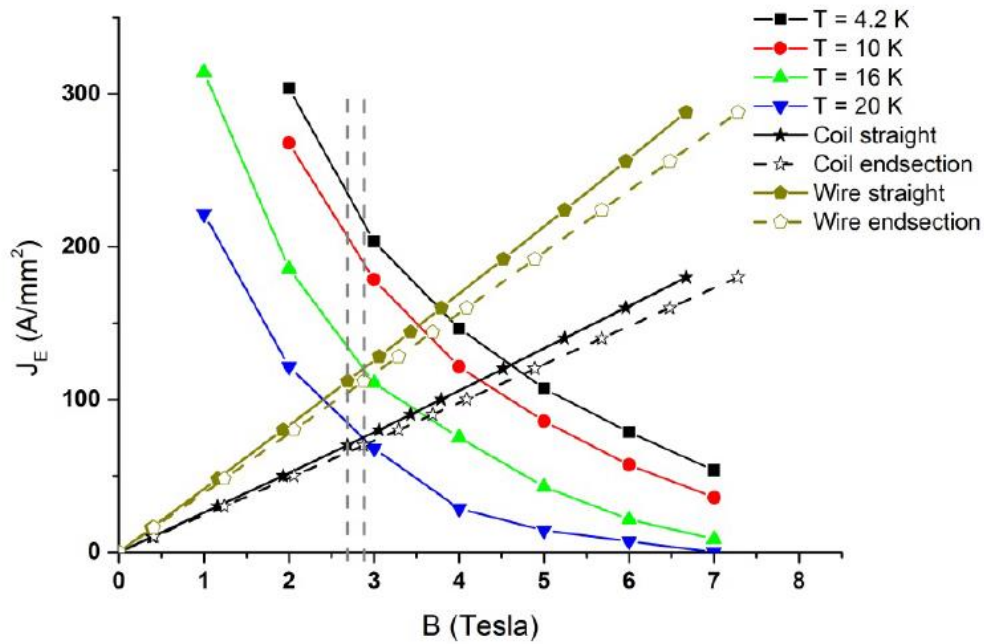


Figure 1.2. Engineering current density of MgB₂ wires at different operation temperatures and the load line of the 10 MW MgB₂ field coils. An operation magnetic flux density just below 3 tesla will demand an operation temperature 16 K < T < 20 K.

1.2 Coil design parameters

The MgB₂ demonstration coil was obtained by scaling the 10 MW generator field winding from a straight section length of 3.1 m and down to 0.5 m as illustrated on figure 1.3. Table 2 is summarizing the properties of the demonstration coil, which is based on a standard 3.0 mm x 0.5 mm MgB₂ wire from Columbus Superconductor.

Table 2. Properties of MgB₂ demonstrator coil being a short version of the field coil of a 10 MW MgB₂ direct drive wind turbine generator.[1]

Length strait section: L_{strait} [m]	0.5	Opening inside pancake: W_{coil} [m]	0.3
Radius of end winding: R_{end} [m]	0.15	Turns in pancake layer: N	100
Thickness of tape: $t_{\text{SC, tape}}$ [mm]	0.7	Width of tape: $W_{\text{SC, tape}}$ [mm]	3.0
Insulation thickness: t_{insul} [mm]	$2 \cdot 0.07 = 0.14$	Space between pancakes: W_{insul} [mm]	1
Coil winding thickness: t_{coil} [mm] ^a	84	Double pancake height: H_{DPcoil} [mm] ^b	7
Tape in pancake: $L_{\text{singlepancake}}$ [m] ^c	220.8	Tape in double pancake: L_{DP} [m]	441.6
Pancake spacing: $L_{\text{coil space}}$ [mm]	1	No. of double pancakes: N_{pancakes}	10
Field coil height: H_{coil} [mm] ^d	80	Total tape usage: $L_{\text{tapetotal}}$ [m]	4416
Field coil width: W_{coil} [mm]	84	Coil filling factor: f_{coil} [%] ^e	62.5

$$^a t_{\text{coil}} = N \cdot (t_{\text{SC, tape}} + t_{\text{insul}}) = N \cdot t_{\text{wire}}$$

$$^c L_{\text{singlepancake}} = N \cdot [2 \cdot L_{\text{strait}} + 2\pi R_{\text{end}}] + 2\pi \cdot t_{\text{wire}} \cdot N(N+1)/2$$

$$^e f_{\text{coil}} = A_{\text{SC}}/A_{\text{coil}}$$

$$^b H_{\text{DPcoil}} = 2 \cdot W_{\text{SC, tape}} + W_{\text{insul}}$$

$$^d H_{\text{coil}} = N_{\text{pancakes}} \cdot [H_{\text{DPcoil}} + L_{\text{coil space}}]$$

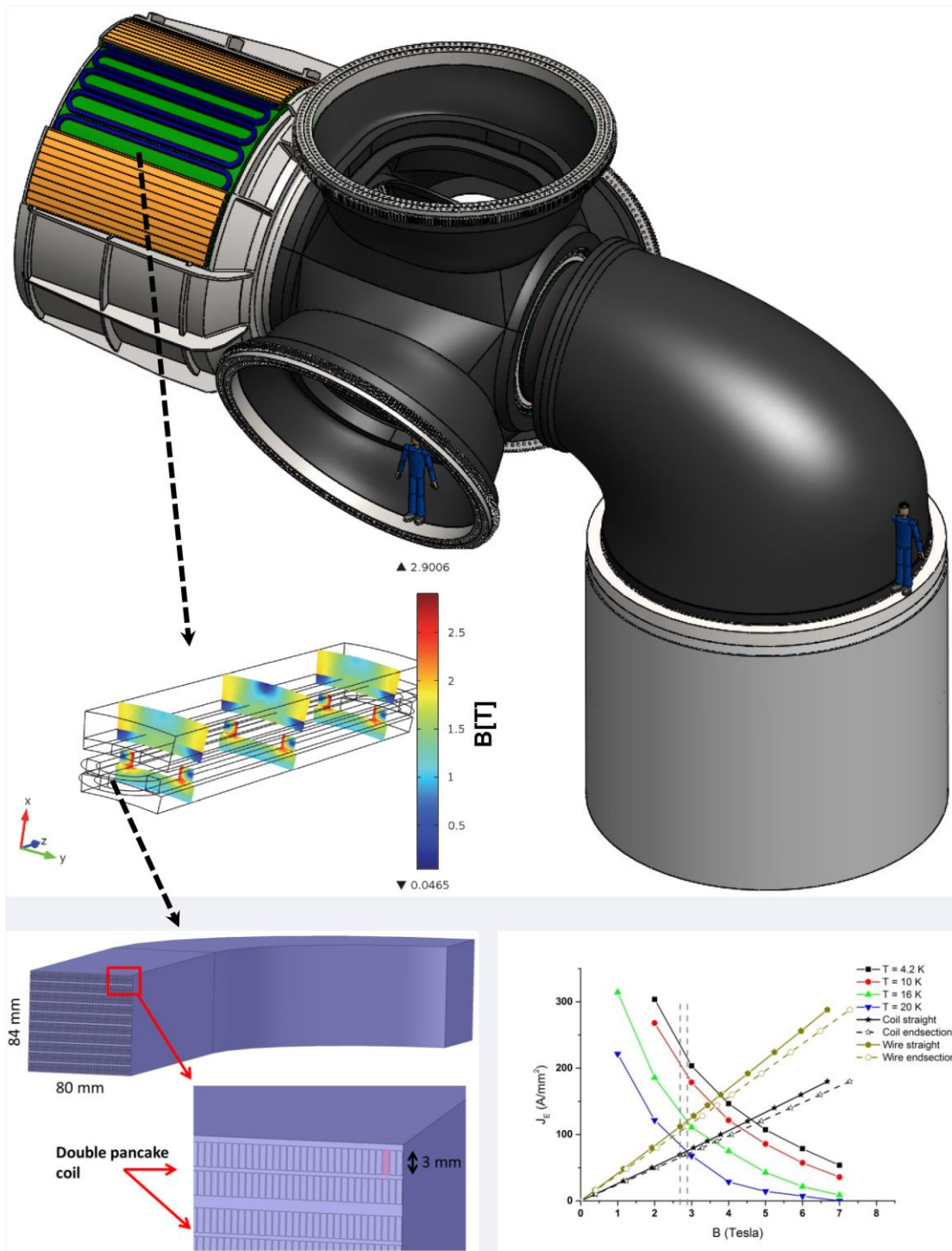


Figure 1.3. Illustration of the layout of the 10 MW MgB₂ direct drive generator mounted in front of the blades of the INNWIND.EU reference turbine and the magnetic flux density of the pole (Top). A quarter of the field race track coil composed of 10 stacked pan cake coils is shown below as well as a zoom into the 100 turns of a 3 mm wire MgB₂ wire in the pan-cake coils. [5].

1.3 Properties of MgB₂ wire from Columbus Superconductors

The MgB₂ wire ordered from Columbus Superconductor [6] in Italy was the standard multifilament wire with 19 MgB₂ filament in a matrix of Nickel and a copper strip soldered

to the side in order to provide thermal and electrical stabilization. Figure 1.4 is showing a Scanning Electron Microscope (SEM) image of the cross section of the wire. The basic wire specifications are

- Nickel external sheath
- 19 Ni filaments
- Filling Factor (FF) 21.5 %
- External Copper stabilization (thickness 0.2 mm)
- Copper Stabilization on one side
- Total Weight: 0.15 g/cm

The dimensions and material compositions are listed in table 3.

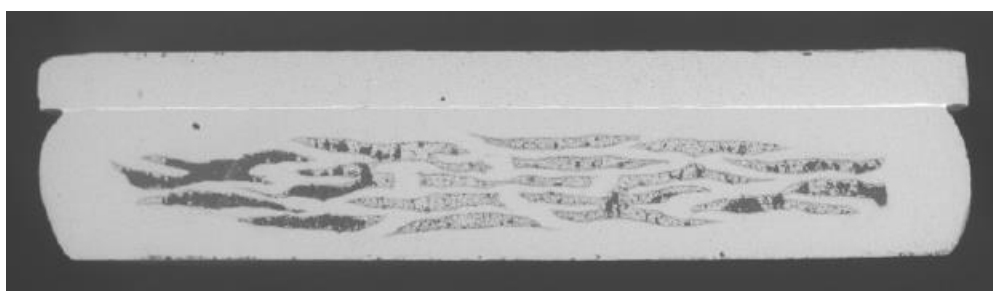


Figure 1.4. Scanning Electron Microscope (SEM) image of cross section of 3 mm wide 19 filament MgB₂ wire with a matrix of nickel (0.5 mm) and a top copper strip (0.2 mm) from Columbus Superconductors [6].

Table 3. Wire dimensions and compositions

Materials	Dimension	%
MgB ₂ [mm ²]	0.34	21.5
Nickle [mm ²]	1.24	78.5
Total wire [mm ²]	1.58	100
Wire cross section [mm]	3.0 x 0.5	
Copper strip section [mm]	3.0 x 0.2	
Total cross section [mm]	3.0 x 0.7	

A total of 4.5 km of wire was ordered from Columbus Superconductors and it was delivered on spools holding up to 1.5 km of length. The first batch was delivered in September 2014 with unit lengths shown in table 4.

Table 4: Critical temperature of September 2014 MgB₂ wire deliverable.

Spool ID	Length [m]	Critical Temperature [K]
V1670	>500	35.2
V1720	>500	35.3
V1727A	>500	35.2
V1727B	>500	35.2
V1735	>500	34.8

Figure 1.5-1.7 are showing the critical current density of the wires in the Sep 2014 batch as function of applied magnetic flux density. The initial target critical current density is

also show as well as a revised critical current criteria reduced by 10 % as agreed upon for the quotation of the wire.

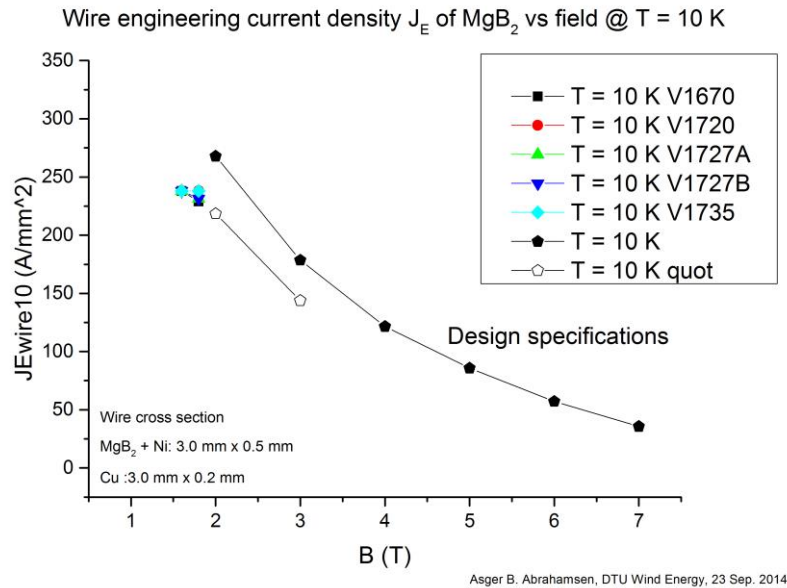


Figure 1.5. Engineering Critical Current density J_E of MgB_2 wires measured at $T = 10\text{ K}$ [6].

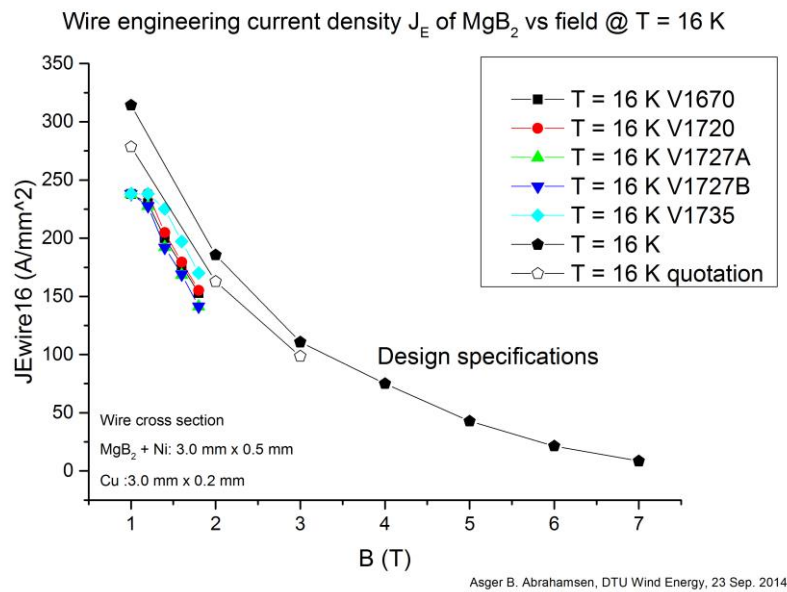


Figure 1.6. Engineering Critical Current density J_E of MgB_2 wires measured at $T = 16\text{ K}$ [6].

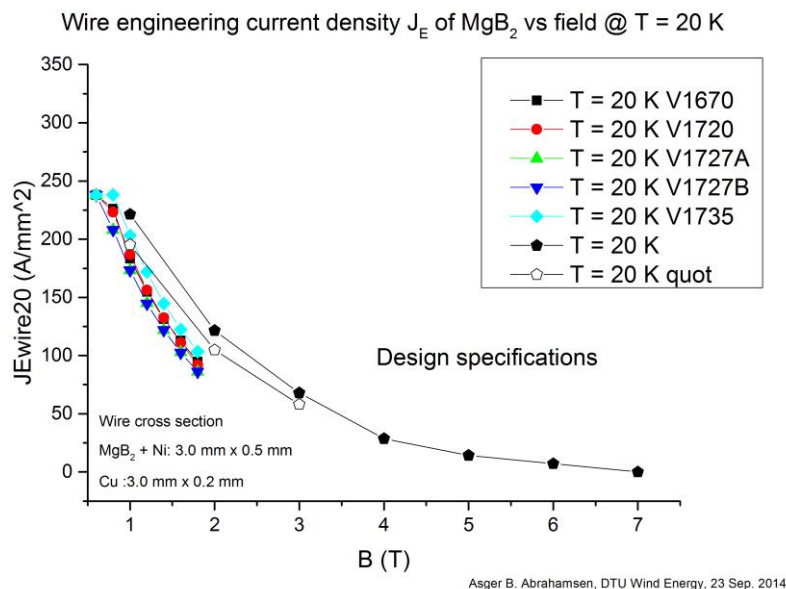


Figure 1.7. Engineering Critical Current density J_E of MgB_2 wires measured at $T = 20\text{ K}$ [6].

Based on the evaluation of the engineering critical current densities shown on figure 1.5-1.7 it was concluded that the delivered wire was not living up to the specification that had been promised in the quotation. After discussion with Columbus Superconductor it was decided that a second batch of wire with improved quality control should be delivered to SINTEF. Table 5 is showing the length, the critical temperature and the critical current of the wire at $T = 20\text{ K}$ and in a magnetic flux density of $B = 1.8\text{ T}$. The criteria for the critical current was set as larger than 220 A at $T = 20\text{ K}$ and $B = 1.8\text{ T}$. According to table 5 it is seen that the wire batch from March 2015 did fulfill the criteria.

Spool	Length [m]	Critical Temperature T_c [K]	IC @ $20\text{ K} \ \& \ 1.8\text{ T}$
V1893	>500	36.3	231
V1922	>500	36.4	239
V1934	>500	36.1	237
V1935	>500	36.1	237
V1936	>500	36.1	247

Table 5. Properties of second batch of MgB_2 wire delivered in March 2015

Figure 1.8 is showing the resulting engineering current density of the selected wires measured up to $B = 1.8\text{ T}$, which is the maximum magnetic flux density of the test equipment of Columbus Superconductors.

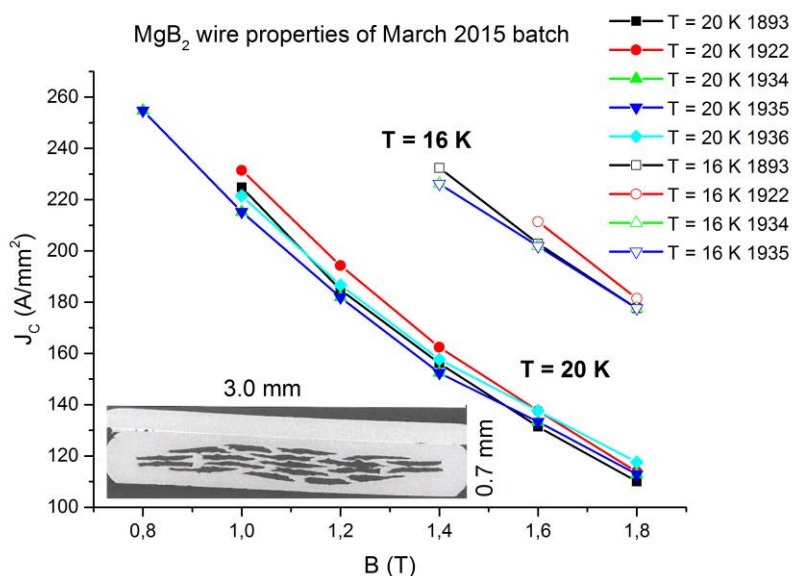
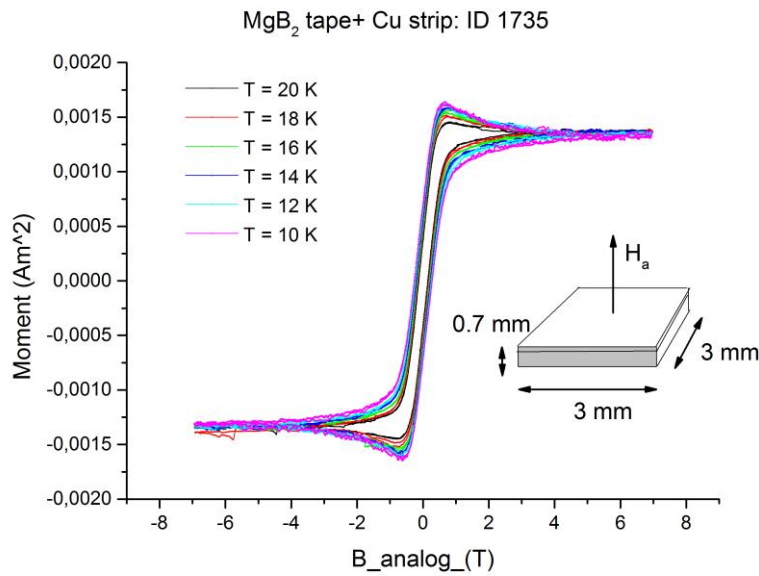


Figure 1.8. Engineering current density of MgB₂ wires from the batch of March 2015.

1.4 Critical current density scaling of MgB₂ wire

A series of magnetization measurements were performed at DTU Wind Energy on 3 mm x 3 mm pieces of selected MgB₂ wires in order to examine if the transport measurements of the critical current density could be determined from magnetization loops obtained at applied magnetic flux densities higher than the 1.8 T limit of Columbus Superconductors.

Figure 1.9 shows a series of magnetization loops of the 1735 wire obtained using a Vibrating Sample Magnetometer (VSM) from Cryogenics Limited. It can be seen that the nickel matrix of the sample results in a ferromagnetic background signal and that the hysteretic magnetization loop of the superconductor is superimposed on that. The opening of the hysteresis loop will be proportional to the critical current density of a superconducting sample according to the simple Bean model [9]. It is however difficult to determine the critical current density in absolute numbers, because the volume of the superconducting phase is not given by a simple geometry (see figure 1.4). Instead one can assume that the critical current density will scale as the opening of the hysteresis loop and then use the scaling factor to scale a critical current as determined by sending a transport current through the superconductor (ex. fig 1.8). Figure 1.10 is showing the scaling of the opening of the hysteresis loop relative to the value obtained for B = 1 T and T = 20 K. Additionally the scaling of the transport critical current of figure 1.8 has been added and it is seen that they are quite similar, which is indicating that the magnetization measurements can be used to examine the field dependence of the critical current density for applied magnetic fields above the characterization range of Columbus Superconductors.



Asger B. Abrahamsen, DTU Wind Energy, Oct 2014

Figure 1.9. Magnetization curves of MgB₂ wire 1735 with the applied field along the tape normal at different temperatures.

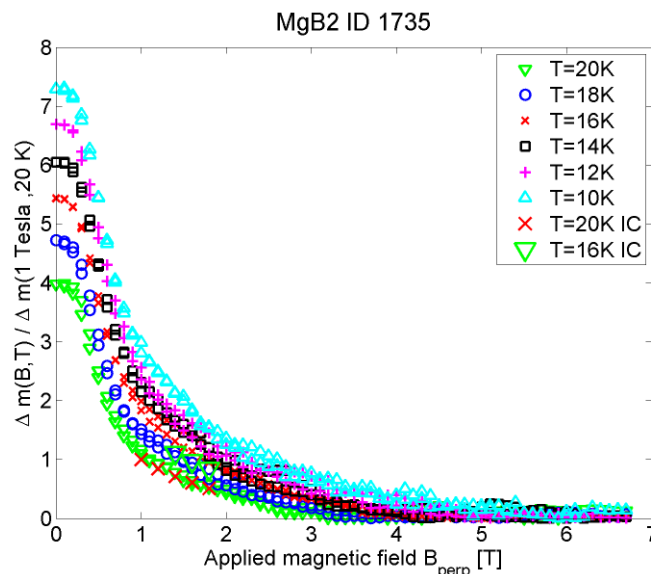


Figure 1.10. Hysteresis opening Δm of magnetization curves of MgB₂ wire 1735 as function of applied field along tape normal and at different temperatures. The opening is proportional to the critical current density J_c of a homogenous sample according to the Bean model [9]. Thus the scaling of Δm with respect to $B = 1$ T and $T = 20$ K is indicating a factor by which the critical current should be scaled.

The magnetization measurements of the properties of the March 2015 batch of MgB₂ wires was tested on 3 mm x 3 mm pieces of that wire used to wind pancake coil no. 2 of the final race track coil. Figure 1.11 and figure 1.12 are showing the hysteresis opening for pieces cut from the two ends of the wire used to wind the pancake coil. It can be seen that a reasonable correspondence with the transport measurements are found again and that an operation point between $T = 15$ - 20 K is confirmed. It should be noted that a comparison of the $B = 0$ T scaling factor for the two pieces of tape is difficult, because the MgB₂ superconductor is known to show thermal flux line pinning instabilities of low field and low temperature, where movement of flux lines is taking place in dendritic

avalanches. Therefore the zero field values will depend heavily on the specific sample characteristics triggering the avalanche process. At higher field $B > 0.5$ T and thereby lower critical current densities, this effect is not as dominant and the comparison between different wires can be done.

The design of the INN WIND.EU MgB_2 demonstration coil is targeting at a rather high magnetic field application of $B \sim 3$ T, because that is the most challenging usage of MgB_2 in a superconducting wind turbine generators. This is following the design philosophy of providing a “light weight and not too expensive” generator. The test of the coil at lower operation current will however also provide insight into a generator design following the philosophy of “Cheap and not too heavy”, where a lot of silicon iron is added to the generator and the magnetic flux density of the superconductor is lowered. It is however important to investigate the upper limit of the coil operation field by determining the scaling of the critical current density in applied magnet field approaching 3 T. Figure 1.13 and 1.14 are showing the hysteresis opening scaling of figure 1.11 and 1.12, but now plotted in a log-scale. What is observed is that the critical current is generally falling off as approximately $J_E \sim B^{-\alpha}$, where the exponent is roughly -1. A transition to a faster decay is however observed for the $T = 20$ K when the applied field is approaching $B \sim 2.5$ T and this might indicate a change in the pinning properties of the MgB_2 superconducting phase. Thus the magnetization measurement indicate that the critical current decay at $B = 3$ T might be larger than what was specified in the quotation of Columbus Superconductors. This is illustrating that further work on quality control of the wires for $B = 3$ T will be useful and that Columbus Superconductors consider their current main market as $B < 2$ T. Additionally optimization of the critical current at $B = 3$ T could most likely be obtained by changing the chemical composition of the MgB_2 by doping with Carbon. Such a development will however call for larger production volumes.

The indication of the faster decay of the critical current as function of field has been used to reconstruct the load line of the MgB_2 demonstration coil, which is shown in figure 1.15. Using a 25 % safety margin to the critical current density of the coil then the current target values in table 6 should be used for the initial test.

Coil temp [K]	$J_{E,critical}$ [A/mm ²]	$J_{E,wire}$ [A/mm ²]	$B_{critical}$ [T]	$I_{operation}$ [A]
5	158	119	3.4	332
10	142	107	3.0	298
15	116	87	2.5	183
20	83	62	1.9	130

Table 6. Suggested MgB_2 coil demonstration test targets based on revised load line and magnetization scaling of the critical current density as shown in figure 1.15 and different temperature of the coil. $J_{E,wire}$ is estimated as 75 % of $J_{E,critical}$.

A systematic measuring campaign of 3 mm x 3 mm pieces of the wires used in the pancake coil is ongoing and will be reported in the final report of the work package. Secondly a transport measurement of the critical current at $B = 3$ T is considered to validate the correspondence between the VSM scaling of the critical current density and the transport measurements.

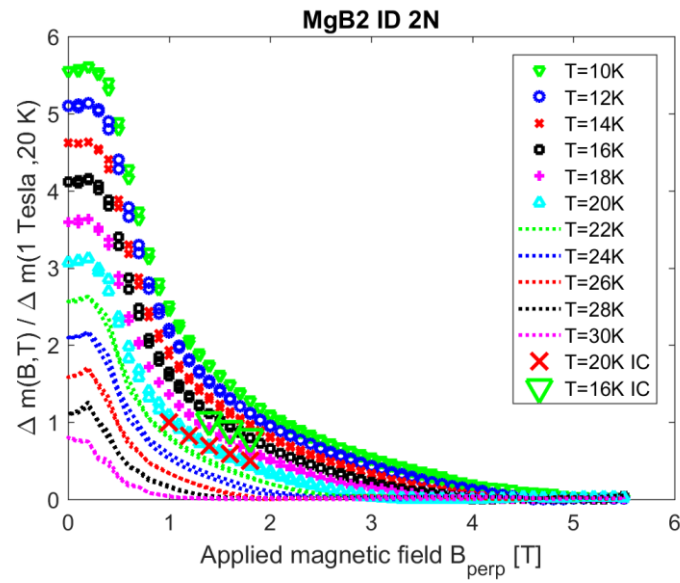


Figure 1.11 Scaling of hysteresis opening of MgB₂ wire at end N of coil No. 2. The transport measurements of figure 1.8 has been added with the last two labels in the legend.

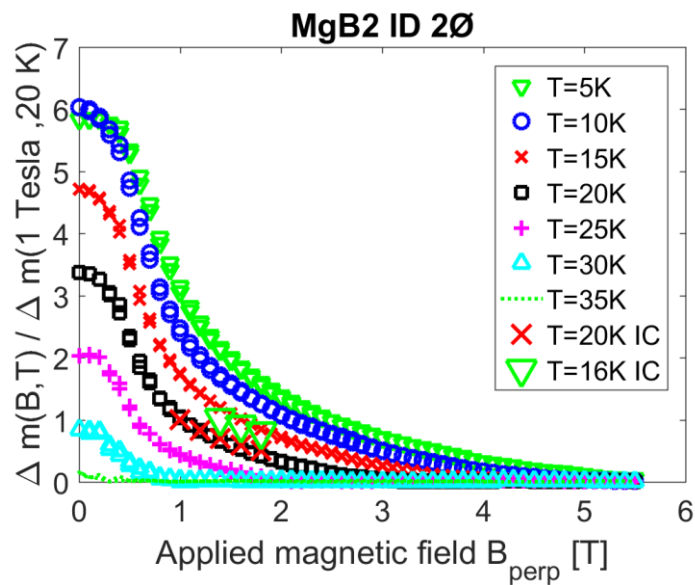


Figure 1.12. Scaling of hysteresis opening of MgB₂ wire at end Ø of coil No. 2. The transport measurements of figure 1.8 has been added with the last two labels in the legend.

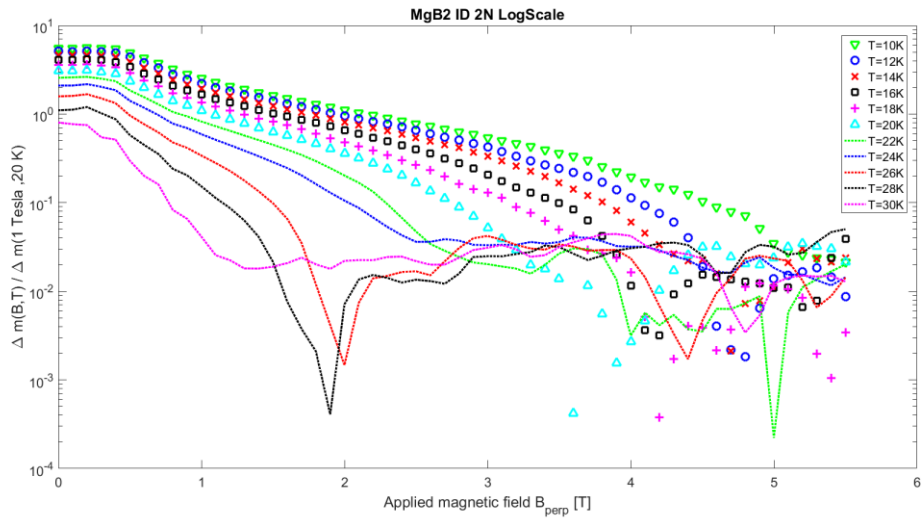


Figure 1.13. Scaling of hysteresis opening of MgB₂ wire at end N of coil No. 2 plotted on a log scale.

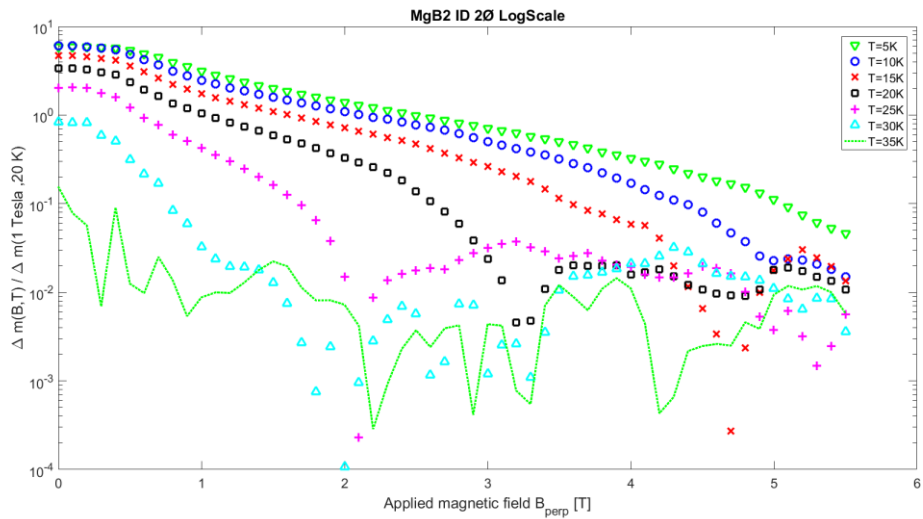


Figure 1.14. Scaling of hysteresis opening of MgB₂ wire at end Ø of coil No. 2 plotted on a log scale.

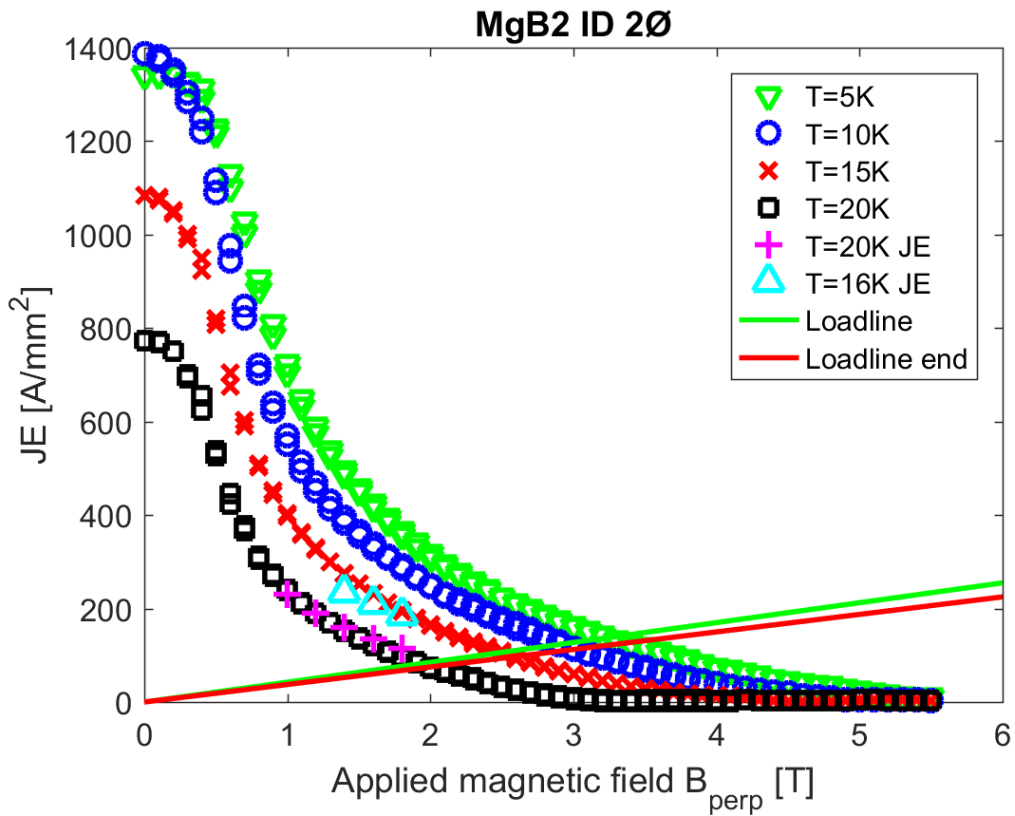


Figure 1.15. Scaling of MgB₂ wire engineering critical current density using the magnetization measurement and the transport critical current measurement for T = 20 K and B = 1 T at end Ø of coil No. 2 plotted on a log scale. The load line of the MgB₂ demonstration coil has been added and the operation points at the different temperature are listed in table 6.

2 WINDING METHODOLOGY

2.1 Wet-winded double pancake coils

MgB₂ superconductors are currently produced in lengths of one to a few kilometres. This is less than what is required for the coil in the 10 MW design. A commonly used method to allow for well controlled splices is to wind so called double pancake coils. The winding procedure starts with the mid part of a wire length, which crosses between a lower and an upper pancake. Half of the wire length is then wound into a lower layer pancake and afterwards the remaining half is wound into an upper layer pancake. In this way the wire ends appear at the outside of the coil and are easily spliced to neighbouring double pancake coils in a low magnetic field and easily cooled region.

An additional advantage with double pan-cake coils is that in case of a failure of one double pan-cake coil, it can be removed or short-circuited, and the remaining part of the coil can be used.

Superconducting windings are normally impregnated with epoxy and can either be dry-wound or wet-wound. In the dry-winding method the conductor is insulated typically with a glass-fibre fabric, then wound into the coil and afterwards vacuum impregnated with an epoxy. In the wet-winding method the conductor is typically insulated with a polymer foil (e.g. Kapton) and then wound while applying a thin layer of epoxy to the conductor sides. An advantage with the dry-winding method is the avoidance of Kapton insulation, which introduces an elastic (and mechanically weaker) component into the superconducting coil. The wet-winding technique on the other hand, allows for winding in a one-step process (avoiding the vacuum impregnation step).

2.2 Epoxy insulated coil

2.2.1 Innovative step

In recent years, non-insulated coils (i.e. without turn-to-turn insulation) have gained significant interest for high-temperature superconducting coils. There are several benefits with non-insulated coils, such as increased compactness and thereby increased overall current density, enhanced thermal stability at quench situations, overall high thermal conductivity of the coil, and avoidance of the so called spongy effect due to differences in Young's modulus between the polymeric insulation and the conductor.

One disadvantage with non-insulated coils is the prolonged ramping time due to the presence of induced currents between turns at high ramping rates. The problem may be reduced or eliminated by the use of a partial insulation between the turns (using a poor conductor between turns or insulating only parts of the windings), thereby increasing the turn-to-turn resistance and allowing for an increased ramping rate. Another disadvantage, for coils such as generator rotors which are operated in the presence of a low ac magnetic field, is that such fields, similarly to the situation during ramping, may induce unwanted ac currents in the coil through turn-to-turn contacts.

In INN WIND.EU we investigate the possibility to use the wet-winding technique without any dedicated electrical insulation except for the epoxy applied to the conductor during winding. In principle, the epoxy gives a sufficiently thick layer for electrical insulation,

however the method needs to be proven and the resistance of possible contact spots needs to be determined and their effect on the coil operation to be evaluated.

In principal, during pure dc operation of a superconducting coil, no turn-to-turn insulation would be necessary. The current is carried loss-free and consequently no voltages would appear between turns, and the current flows only in the superconducting filaments of the wire. However, this is not the case for a coil under real operation. First, the flux flow losses appearing below (but close to) the critical current of the conductor give rise to a small dc voltage over a coil turn. Second, during ramping of the coil, the enclosed flux within the coil changes and consequently a turn-to-turn voltage is induced. If the ramping rate is constant, this voltage is a dc voltage. Thirdly, in a practical wind turbine generator rotor, ac magnetic fields are present leading to induced ac voltages in the rotor winding.

Figure 2.1 shows a cross-section of a test winding. The epoxy layer applied in the wet-winding process constitutes an effective electrical insulation as long as there are no spots incidentally left dry during the wetting process or that the pressure during winding has squeezed the epoxy away at certain points. The uneven top layer is due to long winding time at this first trial winding leading to problems finishing within the pot life of the epoxy. Nevertheless, the test winding can be used to estimate the quality of the epoxy as electrical insulation in the coil.

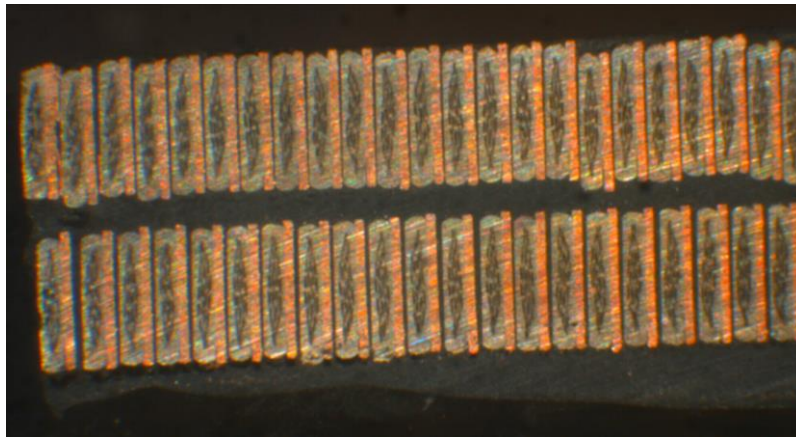


Figure 2.1: Optical microscope cross-section photo of double pan-cake test winding.

2.2.2 Turn-to-turn voltages appearing under operation

Under steady operation, the dc electric field, E_{dc} , along a superconductor operated in the flux-flow region, i.e. relatively close to its critical current, normally follows a power-law dependence according to:

$$E_{dc} = E_0 \left(\frac{I}{I_c} \right)^n,$$

where E_0 is 1×10^{-4} V/m, I is the current in the superconductor, I_c is its in-field critical current, and n is an empirically determined exponent. For an MgB_2 wire operated at a safety margin of 25% and with a typical n -value of 20, E becomes $0.3 \mu\text{V/m}$. For one turn in a 10 MW generator rotor coil the voltage then becomes $2 \mu\text{V}$ since the length of the turn is 6.6 m.

During current ramping, the voltage over the entire coil, U_{coil} , is determined by:

$$U_{coil} = L \frac{dI}{dt},$$

where L is the coil inductance. The inductance of the field winding for the 10 MW generator rotor coil is around 10 H and a typical ramping rate is 0.1 A/s, energizing the coil in 40 minutes. The total coil voltage then becomes 1 V and with 200 turns in the coil, the average voltage for one turn becomes 5 mV. Although varying with position in the coil (somewhat higher at the inner turns and lower at the outer turns) this is the order of magnitude of the turn-to-turn voltage during current ramping.

The space distribution of the magnetic field in the air-gap of the machine contains a fundamental component (sinusoidal distribution) and several harmonics. The harmonics spectrum depends on the design of the rotor and stator. For a stator winding comprising slots and teeth, the harmonic spectrum depends on the number of slots per pole and per phase (q), and if the teeth are magnetic or not. The amplitude of the harmonics becomes larger with magnetic teeth.

When the number of slots per pole and phase q is an integer number, only over-harmonic components are present in the air gap field. They may cause losses in the superconducting field winding if the winding is insufficiently shielded. However, the net flux change and hence the induced voltage in the field winding is small due to the short wavelength of the over-harmonics.

In case of a fractional winding in the stator (e.g. $q=1.5$), there are sub-harmonic components in the magnetic field spanning several poles. They can create a net flux in field winding leading to an ac voltage in the winding. The sub-harmonics can however be reduced by a proper selection of the number of slots in the machine. In addition the frequency is low such that the induced voltage is usually no problem.

To get an estimation of the turn-to-turn voltage we may use the magnetic field distribution calculated for a superconducting generator with non-magnetic teeth. The dominating harmonic frequency in that design is 10 Hz and the (rms) magnetic flux density approximately 3 mT. Now, as this field varies spatially several times over the enclosed area of the field coil, the net flux is maybe one fifth of the area times the magnetic field. The voltage for one turn can then be estimated by,

$$U_{turn} = \frac{d\Phi}{dt},$$

where Φ is the enclosed magnetic flux (equal to the magnetic field times the area). With a total area of the field winding in the 10 MW design of 1 m², the turn voltage becomes approximately 40 mV. It should be noted that this is a very rough estimate only used to get the order of magnitude of the turn-to-turn voltage that could be appearing in the field winding.

Summarizing the turn-to-turn voltages they are of the order 2 μ V, 5 mV and 40 mV for the dc operation, ramping and ac harmonics, respectively.

2.2.3 Turn-to-turn resistance in a double pancake test coil

A double pancake test coil was wound and fed by a dc current of 1 A in room temperature and voltages were measured over approximately one quarter, half, three quarters and the full coil to 1.12, 2.47, 3.58 and 5.04 V, respectively. These numbers reveal no large differences between the quarters of the coil and correspond to the anticipated voltage drops in the wire without large currents passing between turns (and certainly not between the lower and upper layers). It should be noted, though, that the resistance along one turn of the test coil is only about 25 m Ω and for differences in voltages to be detected in these initial measurements, the turn-to-turn resistance needs to approach this level.

To obtain more accurate values on the possible turn-to-turn contact resistance, the coil was cut into four parts and the ends of these parts were sanded (Figure 2.1). The resistances between turns were measured directly (under microscope) using an ohm-meter for values above and a four point method for values below 1 Ω . Several contact points were then detected without any visible contacts at the ends even in the microscope. However, a contact point of the order 1 Ω can be very small and is generally determined by:

$$d = \frac{\rho}{R},$$

where d is the diameter of the contact point, ρ the resistivity of the contact materials (in this case a mixture of copper and nickel) and R the contact resistance. With ρ of the order 2×10^{-8} Ωm and the resistance of the order 1 Ω , the diameter of the contact spot becomes approximately 0.02 μm which is less than what can be seen in a microscope. To eliminate possible contacts at the sanded surfaces, 10 V was applied between turns to burn out any conducting material constituting the contact. For all resistances below 1 Ω the method was effective and sparks could be seen from one of the ends on all samples, showing that the contacts were located at the surfaces (and most likely created during cutting or sanding) and not within the actual coil. For contact resistances above a few Ω the applied voltage had no effect.

In contrast to the low resistance values which were somewhat fluctuating, there were a number of high and stable turn-to-turn resistances. It is likely to believe that these values, which were of the order tens of Ω to several k Ω , are in fact contacts between turns. Their cause may be small particles within the epoxy, imperfections in or metal rest from the wire, or simply that a too thin layer of epoxy was applied, particularly in the second layer of the double pancake test coil where the layers tended to position in a somewhat uncontrolled manner.

Taking the maximum turn-to-turn voltage from section 3.2.2 (40 mV) and the minimum resistance of 10 Ω the current passing the worst contacts can be estimated at 4 mA. This current is far less than the 0.1% of the dc current acceptable from the ac loss point of view [10]. Another question is the power dissipated locally, in this case 0.2 mW, at the contact spot. However, the heat is not generated directly in the superconducting filaments but at the metal surface. The thermal conductivity of the materials will ensure that the heat is conducted both along the wire and through the thin epoxy layer towards the inside of the coil where it is cooled. In fact, if one considers that the heat is conducted in 1 square centimetre from the outermost turn to the inside of the coil, the 0.2 mW corresponds to a temperature increase of only approximately 2 mK.

2.3 Conclusion – winding methodology

Using the epoxy itself as electrical insulation in the wet-winding technique may be a viable and attractive method when winding superconducting coils. A test wound coil showed no low resistive contacts, and it is likely that an all through well controlled winding process would increase any contact resistances further. By avoiding a dedicated electrical insulation, like Kapton, the cost is reduced (the insulation cost is about 10% of the cost of the MgB_2 wire), one step in the coil manufacturing process is removed, and maybe most importantly, the radial thermal conductivity of the coil increases dramatically.

The wet-winding technique with the epoxy itself as electrical insulation is chosen for winding double pan-cake coils for the INN WIND.EU MgB_2 demonstrator coil [2]

3 COIL WINDING AND ASSEMBLY

3.1 Winding procedure

The MgB_2 superconductor is delivered by Columbus Superconductors on cable drums with a length of either 500m or 2000m[6]. These cable drums are unsuitable for winding and therefore, the superconductor was first wound from factory drums onto special cable discs. When doing this the cable drums were mounted onto a pole for unwinding as indicated in Figure 3.1. While winding the required amount of 500 m from a factory drum onto a cable disc, the tape passed through a device which measured the tape length.

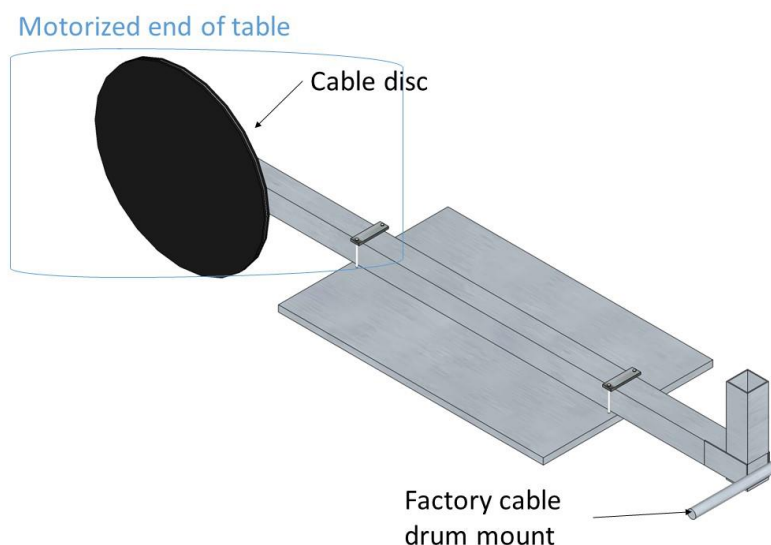


Figure 3.1: Winding table in vertical position for winding the tape onto the table discs.

When the sufficient length of superconductor was wound onto the cable disc, the winding table was turned to a horizontal position. The mold was then placed at the motorized end of the table. This mold was smeared with Emerson & Cuming mold release 122 S to ease the removal of the coil when the epoxy had hardened. Placement barriers were attached to the mold to ensure that the superconducting tape is placed in a correct manner, see Figure 3.2.

To wind a double pancake coil one has to start winding at the middle of the wire to use one half for the lower layer and the other half of the upper layer. Therefore, half of the conductor was wound onto a second cable disc. This cable disc was placed on top of the mold before the tape was wound onto it as illustrated in Figure 3.3.

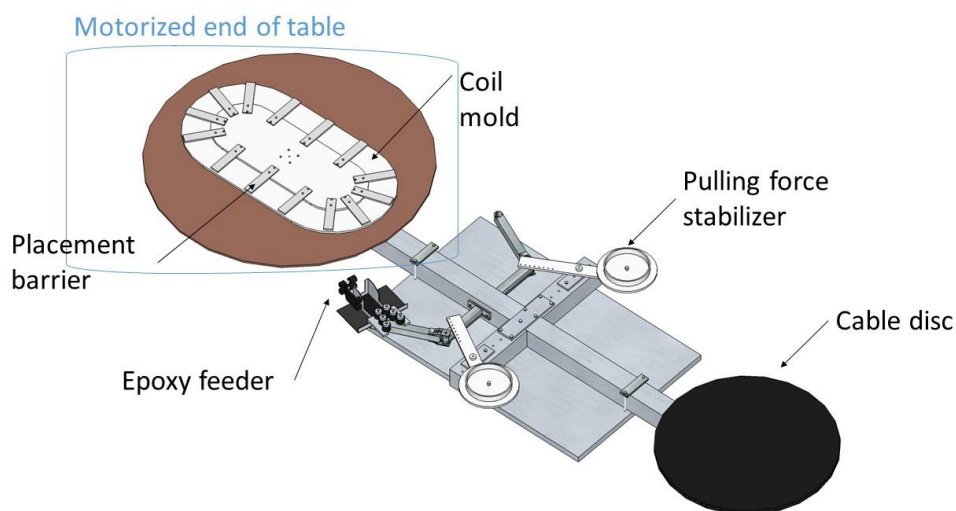


Figure 3.2: Winding table in the horizontal position.

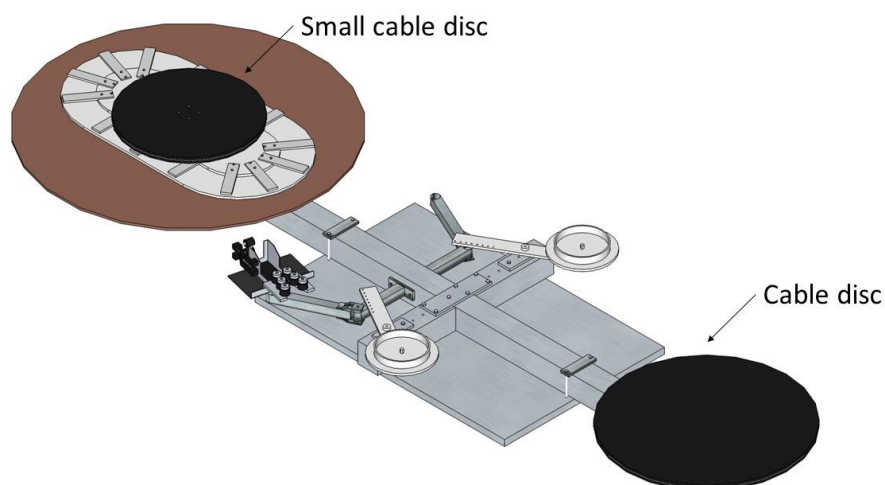


Figure 3.3: Winding table with attached discs.

The table was a pulling table, which means that one side had an engine and the other had a break. This break was adjusted such that the pulling force was approximately equal to tensile stress of 20 MPa. A counter was mounted underneath the rotating mold to keep track of the number of turns.

The actual winding process started with the mixing of alumina filled Epoxy Stycast 2850 and hardener catalyst 24LV (weight-ratio = 1:0.07). The composition must be mixed properly for approximately 5 minutes. The superconductor was then placed inside the epoxy container, and the epoxy was poured into it. Then the winding commenced. The winding speed was for the first turn slow with multiple stops to get a controlled transition between the upper and lower layers (as a double pancake starts at the middle with this transition). When the tape settled nicely, the speed was increased.

The process was carefully monitored in case of irregularity occur. The winding speed was reduced during the winding of the last turns of the lower layer. When the lower layer was wound, the tape was cut and fastened to the table.

When the first layer of the double pancake coil was wound, some intermediate preparations were necessary before winding the upper layer to complete the pancake coil. The second cable disc was carefully moved from the mold to the opposite end of the table. The placement barriers were then removed. If the appliance of epoxy had been too generous, excess epoxy was removed. Shim plates made of stiff epoxy was evenly distributed on top of the lower layer as shown in Figure 3.4 (to avoid electrical contact between layers).

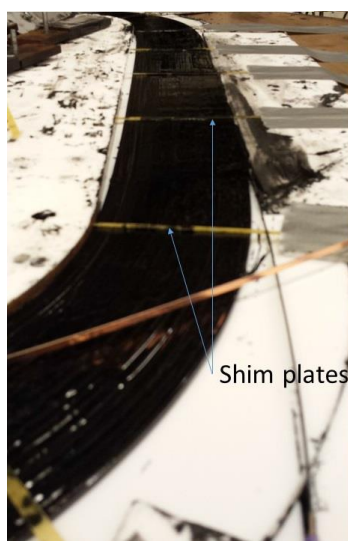


Figure 3.4: First layer with shim plates.

Placement barriers for the upper layer were mounted on the table. A second batch of epoxy was mixed and then the winding of the upper layer commenced in the same way as for the lower layer.

When both layers were wound, the windings of the straight section were pressed inwards until the width of the coil section was 84 mm. A small length of superconductor was attached to the outgoing connections for mechanical support, since this is the weakest points of the coil. To ensure that the turns did not have any height deviations, downwards pressure was manually applied on top of the shim plates to even out any irregularities. Excess epoxy was removed before adding a mold that fitted on top of the coil. Weights were added for downward pressure and the coil was stored over night for hardening of the epoxy. The next day the equipment was disassembled and the pancake coil was carefully removed from the mold, inspected for damages and placed onto the thermal interface as shown in Figure 3.5.

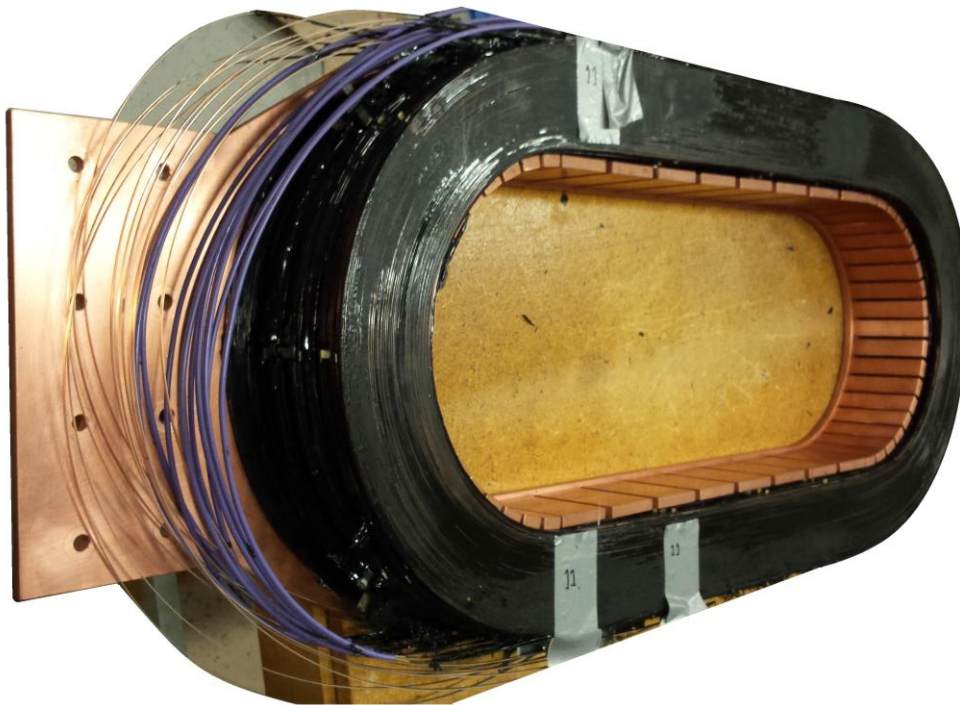


Figure 3.5: Double pancake coils stored on the thermal interface.

3.2 Assembly of sub-coils

The ten individual coils, wound as double pancakes, needed to be assembled, both electrically and mechanically. The assembly was done in steps where one coil was first glued with epoxy and then joined electrically with the previous coil by soldering. This procedure was repeated until all of the ten coils were connected. The epoxy used was Stycast 2850 FT mixed with the hardener Catalyst 24 LV (weight ratio 1:0.07). This is the same epoxy used for turn-to-turn insulation. The solder used was Almit SR-37 LFM-48S and it consists of 96,5% tin, 3% silver, 0.5% copper and some trace elements for reinforcement. The melting point of this solder was 217°C.

The first coil was glued on a thermal interface made of copper. The thermal interface will be connected to the cold head, and cool down the coil more effectively. The interface is also the mechanical structure that keeps the field windings together during assembly. It is made by a copper plate with the shape of the coils, with an additional space on top to connect the cold head. Copper teeth are mounted on the inner edge to fit each individual coil. The teeth will make the coils line up on top of each other and increase the cooling surface to the coil. The bottom of the thermal interface is shown in figure 3.6.



Figure 3.6: The bottom of the thermal interface with all the copper teeth mounted on the inner edge.

An identical copper plate was placed on top of the coil to increase the thermal conductivity. Every other copper tooth seen in Figure 3.6 was mounted on this plate, to distribute the cooling better and more even. The teeth are lower than the field winding to prevent an electrical connection between the two plates, which otherwise would have resulted in induced currents between the plates when the current is ramped during testing.

During the assembly of each coil, every tooth was mounted on the copper plate at the bottom as seen in Figure 3.6. This was necessary to ensure that less epoxy would drain, but also leave a perfect groove for the teeth when they were mounted on the top plate. Every other copper tooth was therefore covered with a regular cling film to prevent them from attaching the epoxy. The other half was covered with Kapton tape for electrical insulation between the field winding and the copper teeth.

Pieces of fiberglass were placed between the interface and the first coil to prevent an electrical connection. The pieces were 0.4 mm thick and were distributed around the thermal interface as seen in Figure 3.7. The fiberglass pieces were also placed between the coils to prevent shorting any turns from one coil to the next.

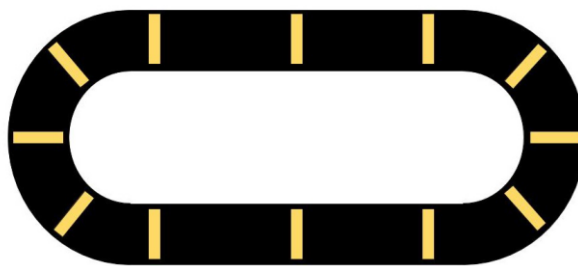


Figure 3.7: Placement of the fiberglass pieces between the individual coils.

Epoxy was applied to the thermal interface and at the bottom of the first coil. Before the epoxy was added to the bottom of the first coil, cavities between the wires from the winding procedure was refilled. A small portion of epoxy was heated in a water bath to make the viscosity lower such that the epoxy would drain more easily. This made the epoxy able to drain into the cavities and fill them. After both surfaces were covered with a layer of epoxy, the coil was flipped and placed on top of the thermal interface. The coil was pushed down by adding weight on top of it. This was done to minimize the layer of

epoxy and to make sure that there were no gaps between the coil and the thermal interface. A 20 mm thick piece made of Teflon, shaped similar to the coil, was placed on top of the superconductor wires, and 10 kg weights were placed on the Teflon plate as seen in Figure 3.8.

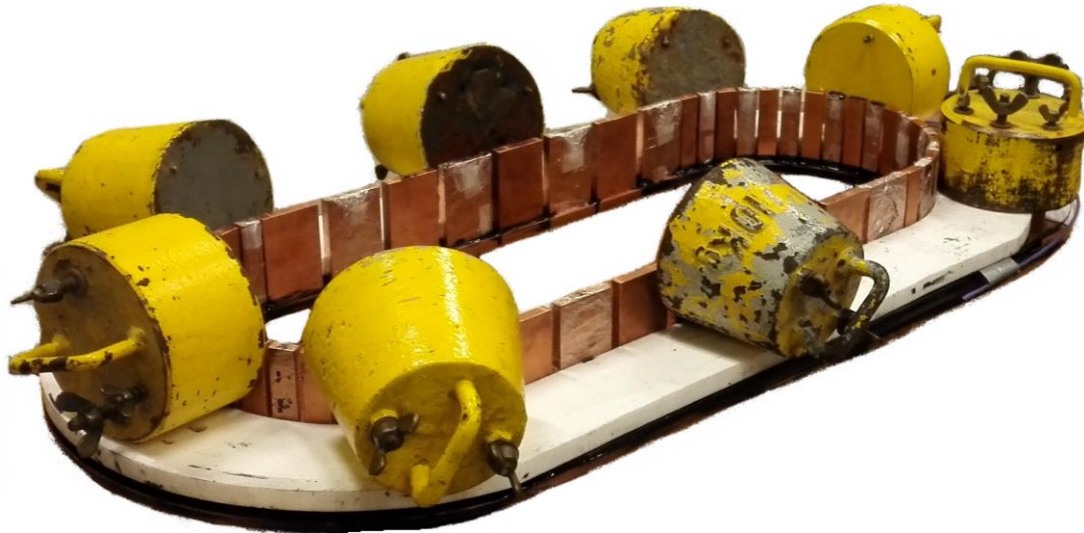


Figure 3.8: The first coil glued to the thermal interface with Stycast 2850 FT. The layer of epoxy was minimized by adding weight on top of the coil to push it down.

The epoxy had a cure time of 16-24 hours in the room temperature of 25 °C. The weights stayed on the coil during the night and were removed the next day when the epoxy had cured. The next coil was added on top of the first coil by doing the same procedure as described above.

One problem that occurred was that all the individual coils were leaving a gap between the copper teeth along the straight edge. In other words was the inner edge of the coils not perfectly shaped to the straight alignment of the copper teeth on the thermal interface. The gaps were filled up with pieces of superconductor and extra epoxy, as shown in Figure 3.9. In this way the same material properties were present here as in the rest of the coil.



Figure 3.9: The pieces of superconductor that were placed between the tenth coil and the copper teeth.

When the second coil was glued and the epoxy was hardened the first joint was made by soldering. The soldering technique is described in detail in Section 3.3. Figure 3.10 shows the soldering of two double pan-cake coils.



Figure 3.10: The first and second coil soldered together.

3.3 Soldering

At the overlap joints between double pan-cake coils the current passes metal in its normal state and joule heating appears. To avoid large heat loads to the cooling system and hot spots potentially jeopardizing the operation of the coil, the resistance of the joints needs to be kept low.

A two-step soldering method was applied. First, the two ends of the MgB_2 conductors were pre-soldered (Figure 3.11) on their copper respectively nickel sides, and secondly the ends were soldered together using a specially developed tool (Figure 3.12). For the first step the key is to find a good choice of solder and soldering temperature for the solder to both wet on the two different surfaces and not to delaminate the copper strip from the nickel matrix of the wire. Additionally, for healthy reasons and regulations, a lead based tin should be avoided.



Figure 3.11: Pre-soldering of copper (left) and nickel (right) sides of the MgB_2 superconductor.

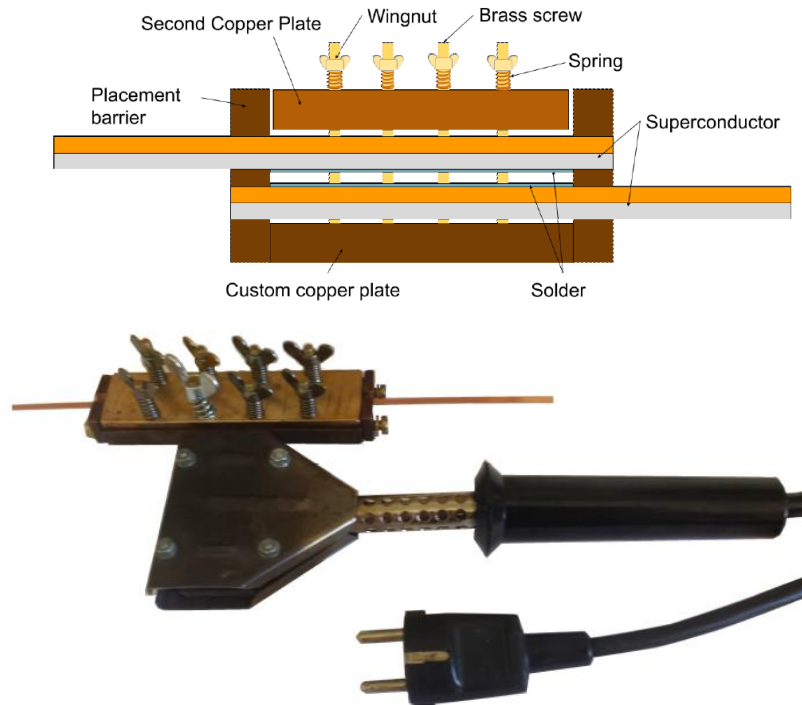


Figure 3.12: Soldering tool, principle (left) and actual tool (right).

Before pre-soldering, the surfaces of the conductors were sanded (using P800) to remove oxides from the metal and isopropanol was used to obtain a clean surface. Pre-soldering was then performed with the lead-free solder Almit SR-37 LFM-48S. As the superconductors are joined with an overlap, pre-soldering was performed on the copper side on one end and on the nickel side of the superconductor on the other end of the joint. A regular temperature controlled soldering iron with a set temperature of 250°C was used for the pre-soldering.

A high power soldering iron was modified to solder the pre-soldered ends together. The iron tip was replaced by a custom made copper mold. As displayed in Figure 3.12, the mold is composed of a massive copper plate with brass screws and placement barriers. A second copper plate is threaded down the screws equipped with springs and attached. The springs apply pressure while soldering such that the layer of solder becomes thin, and hence the resistance of the joint becomes low.

The pre-soldered superconductors were placed in the soldering tool with their copper sides facing up. The wires overlapped and were held in place by the placement barriers at each end of the soldering tool. Then the copper plate was placed on top of the joint and the screws with wingnuts were compressed. A maximum temperature of 290-300°C was applied for the solder to liquefy such that the springs could compress the layer of solder to a minimum.

The method was validated by studying the thickness of the solder between the joints in an optical microscope (Figure 3.13). The solder layer thickness of less than 5 µm is considerably smaller than the nickel layer the current also has to pass. A final test of the resistance of the joints had to be made when cooled down and was performed during the initial testing of the full coil (chapter 5).



Figure 3.13: Optical microscope cross-section view of soldered joint.

4 TESTING PROVISIONS

4.1 Mechanical support

Due to the magnetic field and current in the superconducting coil, there is a substantial force acting on each wire in the coils. The force acts normal to both the magnetic field direction and the current, giving a force acting "radially" outwards on the wires. The superconducting wire has a limited mechanical strength, and, hence, mechanical support of the coils is needed. In particular the straight sections of the racetrack of the coils need additional support.

The force acting normal/perpendicular to the straight sections of the coils in the racetrack was calculated to be approximately 400 kN. To support the straight sections of the coil a mechanical support consisting of two stainless steel plates spanning the coil together with two thicker stainless steel plates covering the gap and supporting the straight sections of the coil. When dimensioning the mechanical support, it was assumed that the full force acted on the mechanical support. In reality, the copper thermal interface and the coils themselves have mechanical strength, which means that there is some redundancy in the mechanical strength of the complete assembly.

The material for the mechanical support was stainless steel of the grade 316LN, chosen based on previous published work on the cryogenic properties of the different steels grades. Grade 316 LN has low magnetic permeability and limited adverse mechanical qualities (tensile strength, fatigue life etc.).

When dimensioning the mechanical support the total deformation of the mechanical support was calculated. A value for the maximum deformation of the straight section of coil in the racetrack was used as a benchmark. The mechanical stress in the large plate becomes $\sigma = F/2Lt = 400 \text{ kN}/(2 \cdot 0.5 \text{ m} \cdot 0.005 \text{ m}) = 80 \text{ MPa}$, well below the yield stress for grade 316 LN stainless steel at cryogenic temperatures. For a Young's modulus of 210 GPa, the strain becomes 0.04%, and the elongation of the 0.5 m wide plate becomes approximately 0.2 mm.

The thicker steel plate directly supporting the coil is deformed by bending, and the maximum deformation of a 20 mm thick plate with a width of 90 mm is 0.003 mm. Thus, if the additional mechanical support is to take the full force, a maximum deformation along the straight part of the racetrack will be 0.1 mm + 0.003 mm = 0.103 mm. The installed mechanical support around the coils is shown in Figure 4.1.



Figure 4.1: Mechanical support mounted on the coil.

4.2 Cooling - redesign of cryostat for the particular coil

The cryostat used for testing the coil was originally designed and built for testing of circular superconducting coils and borrowed from Tampere University of Technology, see Figure 4.2. The coil is placed in vacuum inside the stainless steel cryostat. Cooling is supplied by a cooling machine with a two-stage cold head inside the cryostat. The low-temperature stage (10-20 K) of the cold head cools the coil, whereas the high-temperature stage (40-80 K) cools a radiation shield surrounding the coil.

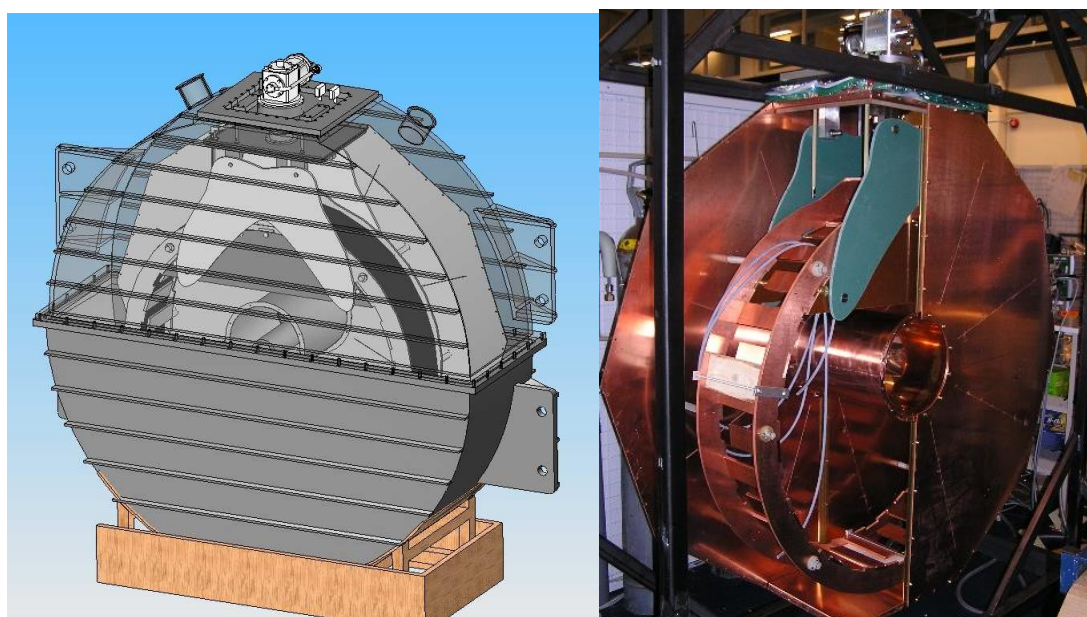


Figure 4.2: Original cryostat. Left: Schematic drawing of the cryostat with circular coil. Right: Circular thermal interface and copper radiation shield. Courtesy Tampere University of Technology.

To facilitate testing of the racetrack shaped INN WIND.EU MgB₂ coil certain adjustments were needed. First of all, a new thermal interface was needed. The thermal interface connects the coil to the cold head of the cooling machine. Figure 4.3 shows the interface during construction. Copper teeth are mounted on two copper plates (only one of them seen in Figure 4.3, the other one is placed on top of the copper teeth). During cool-down, the heat is withdrawn from the coil to the cold head of the cooling machine.

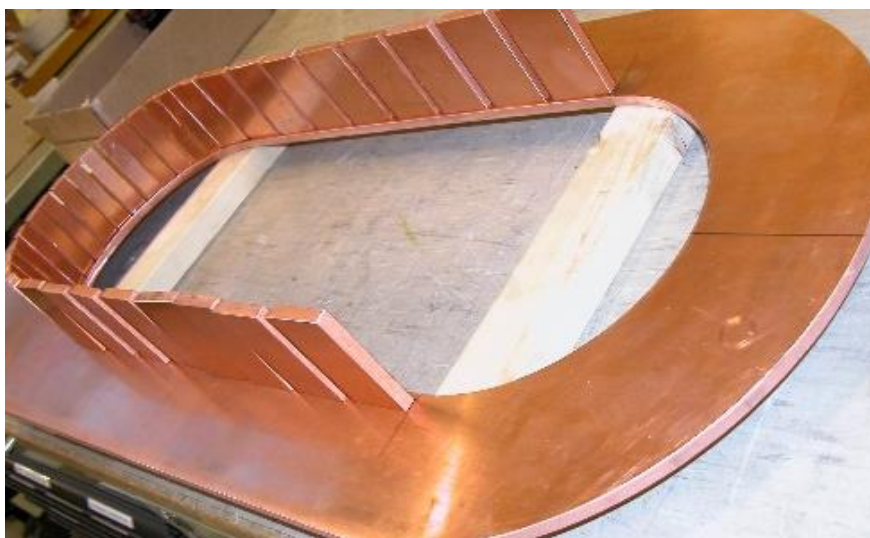


Figure 4.3: Half of the thermal interface during construction.

The large copper plates are connected via flexible (to allow for thermal contraction during cool down) copper sheets to the cold head (Figure 4.4, left). The weight of the coil, the thermal interface and the mechanical support is taken up by glass-fibre reinforced epoxy plates mounted to the outer cryostat wall at the top of the cryostat (Figure 4.4, right).

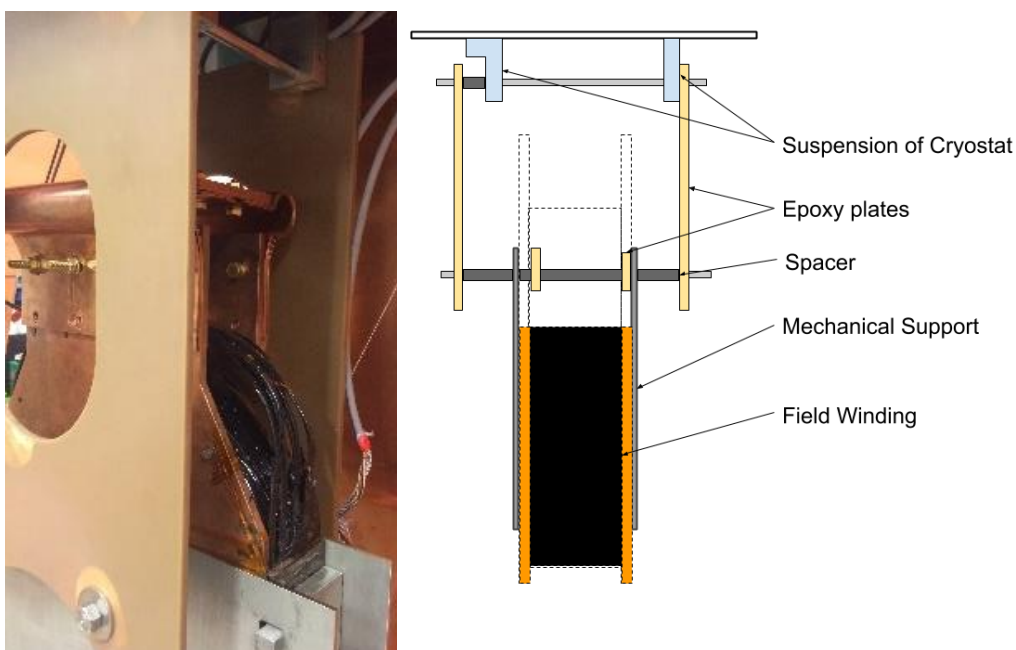


Figure 4.4: Left: Top of coil with thermal connection to the cold head and mechanical connection to the top of the cryostat. Right: Schematic of the suspension system.

The cryostat walls are, due to the compressive vacuum forces, supported by stainless steel bolts. Since the mechanical support occupies the centre of the cryostat, two bolts were used, one on each side of the coil. The radiation shield was reconstructed accordingly (Figure 4.5).

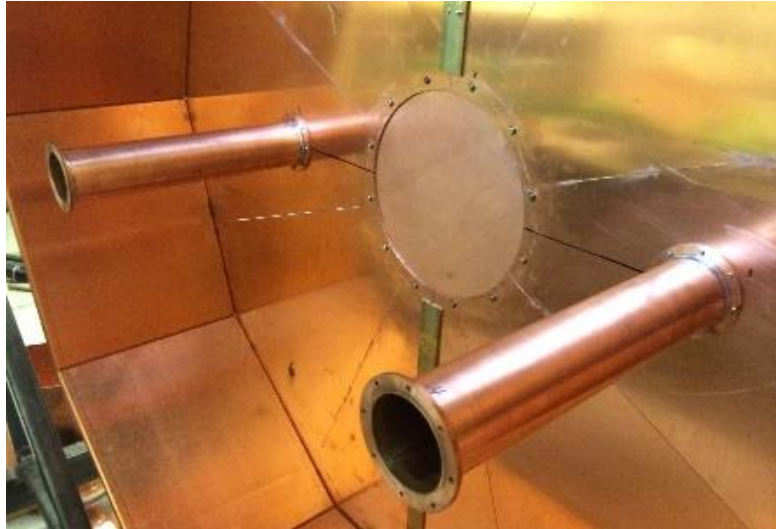


Figure 4.5: Reconstructed radiation shield.

4.3 Current leads

Current are conducted to the coil through current leads. Between room temperature and the second temperature stage (40-80 K), copper and brass current leads are used. To limit the thermal leakage into the coil, high-temperature superconductors (HTSs) are used between the second temperature stage and the coil. A BSCCO HTS tapes from Sumitomo, with a critical temperature of 110 K and a good current carrying capability for temperatures below 80 K, were used. Three wires in parallel were soldered on each end to be sure that the current in each wire would not exceed the critical current at the operating temperature and magnetic field. An estimated temperature of around 66 K based on measurements from previous use of the cryostat, and a magnetic field of 0.25 T were used to find the critical current of the HTS tapes. The magnitude of the magnetic field was based on simulations in COMSOL multiphysics. These numbers represent a worst case scenario, where the hottest spot would be where the highest magnetic field is present. In reality the coldest spot of the HTS is where the highest magnetic field is present and vice versa. Based on the worst case scenario, the BSCCO tape has a critical current of approximately 100 A. To be able to conduct 200 A with some safety margin, and to allow for testing at higher currents, three wires were chosen. Figure 4.6 shows the HTS tapes.



Figure 4.6: HTS tapes between the coil and the second temperature stage.

4.4 Quench protection

If, for some reason, a part of the superconducting coil goes from the superconducting state to the normal state, the resistance increases and heat is generated. This is called a quench and if the heat increases too much or too fast, a quench can damage the superconducting coil. To avoid such damage, a quench protection scheme is chosen. Generally the magnetic energy stored in the superconducting coil needs to be released in a controlled way, preferably as heat in a resistor outside the cryostat.

The schematic of the chosen quench protection is shown in Figure 4.7. In normal operation, the switch is closed. The current source energizes the coil. The resistance R_1 (5 – 50 m Ω , the lower value for higher currents (200 A)) enables stable operation in controlled voltage mode. The resistance R_2 (1-2 Ω) is used to take up the energy if a quench situation occurs. To release the energy in R_2 , the switch has to be opened.

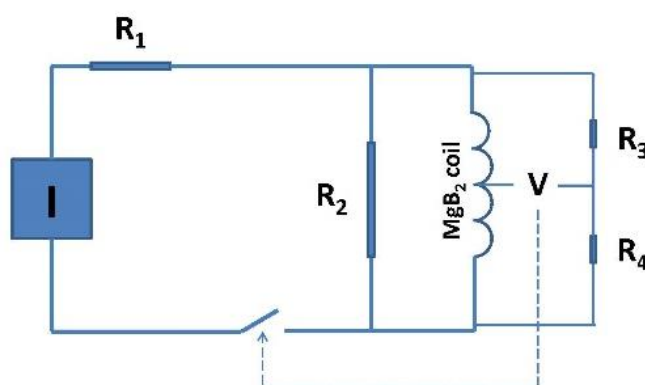


Figure 4.7: Quench protection system.

To control the switch a bridge coupling is used where the voltage V becomes zero with the right choice of R_3 and R_4 (R_3 and R_4 being almost equal). If a voltage appears in the MgB_2 coil, an imbalance occurs and V increases. When V passes a predefined limit, a signal triggers the switch to open.

For the approximately 5 H INNWIND.EU coil, the stored energy at 200 A becomes 100 kJ ($1/2 \cdot L \cdot I^2$). This energy should, in case of a quench, be taken up by R_2 . For this Kanthal resistance tapes can be used. Twenty metres of 1.5 mm x 10 mm Kanthal tapes have a resistance of approximately 2 Ω . When 100 kJ is dissipated in the tape, its temperature rise becomes below degrees centigrade.

4.5 Magnetic field safety

During testing, the coil generates a significant magnetic field. Strong DC magnetic fields may violate the operation of e.g. pacemakers and a safety distance from the coil needs to be established. International standards set the acceptable limit to 0.5 mT. Based on FEM-calculations, Figure 4.8 gives the safety distance as function of current in the coil.

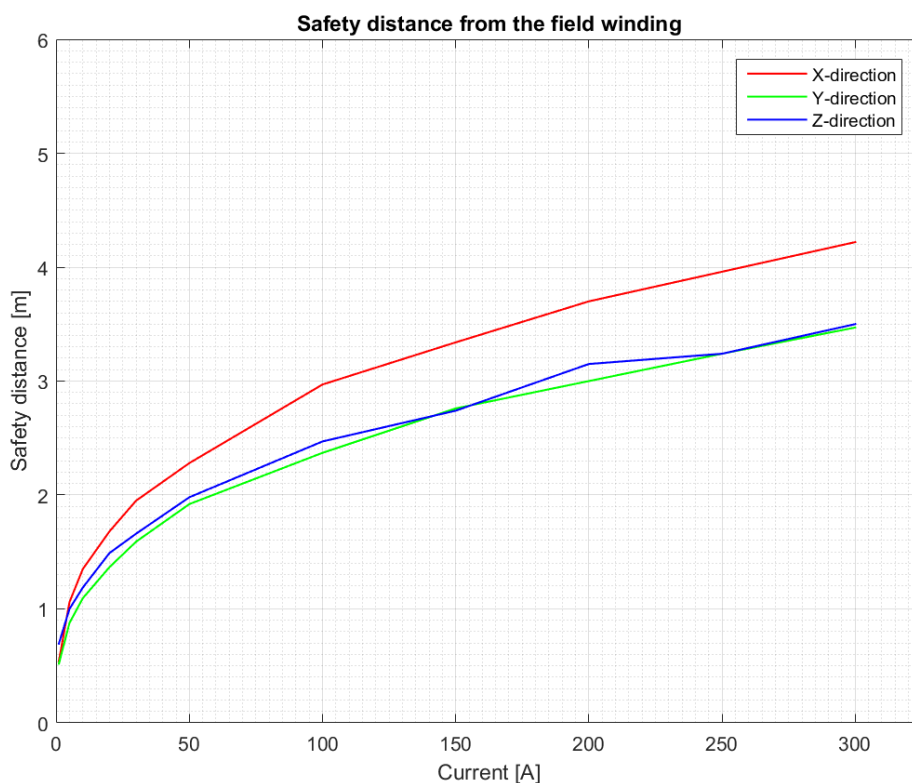


Figure 4.8: Safety distance from the centre of the coil as function of current. The x-direction is perpendicular to the plane of the coil, the y-direction is oriented perpendicular to the straight section of the coil, and the z-direction is oriented parallel to the straight section of the coil.

5 INITIAL TESTING

The coil was inserted in the cryostat which was evacuated for four days with a rotary vane vacuum pump before a turbo molecular vacuum pump was switched on to bring the pressure down below 10^{-4} mbar to practically eliminate heat conduction through the gas. Figure 5.1 shows the cryostat with vacuum pumps.

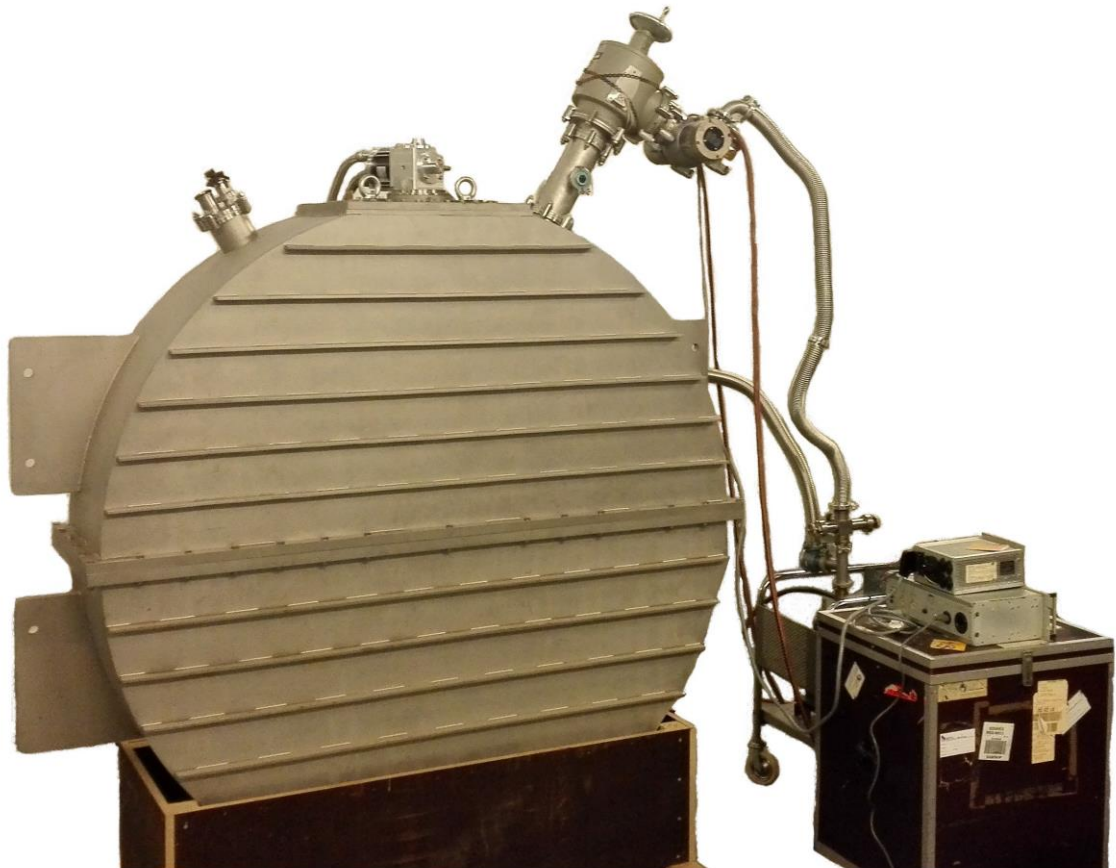


Figure 5.1: Assembled cryostat during evacuation.

The cooling machine was switched on. The temperature, measured with Cernox sensors, during cool down is shown in Figure 5.2. The blue line represents the sensor placed on the thermal interface near the cold head, whereas the red line represents the sensor placed at the bottom of the coil (see Figure 5.3). The cool down time was approximately 7 days before the temperature stabilized at 18 K at both sensor positions.

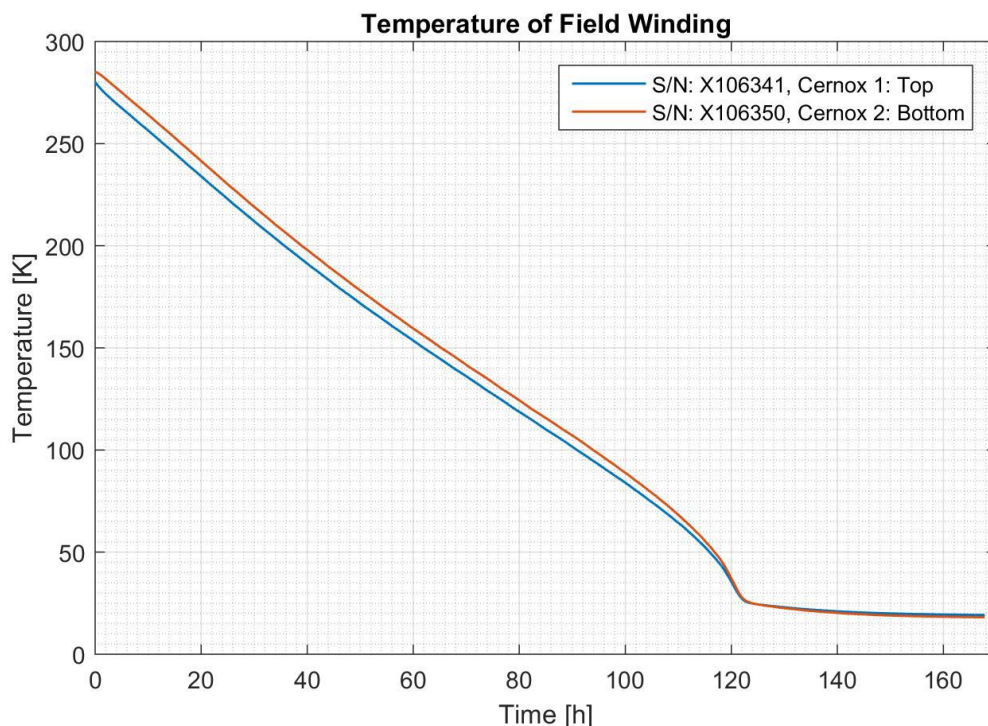


Figure 5.2: Temperature of the coil during cool down.



Figure 5.3: Sample holder for bottom Cernox sensor at the bottom of the cryostat furthest away from the cold head.

When cooled down, current was injected in the superconducting coil and ramped in different sequences to different currents of maximum 16 A. The ramping rate was varied between 0.01 A/s and 0.1 A/s (0.05 V to 0.5 V over the coil). Figures 5.1-5.3 show the results when the current was ramped to 16 A, with intermediate stops where the current was stabilized to enable voltage measurements.

Figure 5.1 shows the voltage drop over the BSCCO/Ag HTS current leads. These superconducting current leads show a substantial voltage already from the lowest current, indicating a resistive part and malfunction of the current leads. HTS 1 and HTS 2,

representing the current leads on each side, show a similar behavior. This fact indicates a problem with cooling rather than with poor superconductors. The resistance at low currents corresponds to a normal zone of the HTS current leads of 0.1 - 0.2 m of the approximately 0.6 m long current leads. The problem with the current leads obstructed testing at higher currents as possible burn out of the current leads could set equipment at risk.

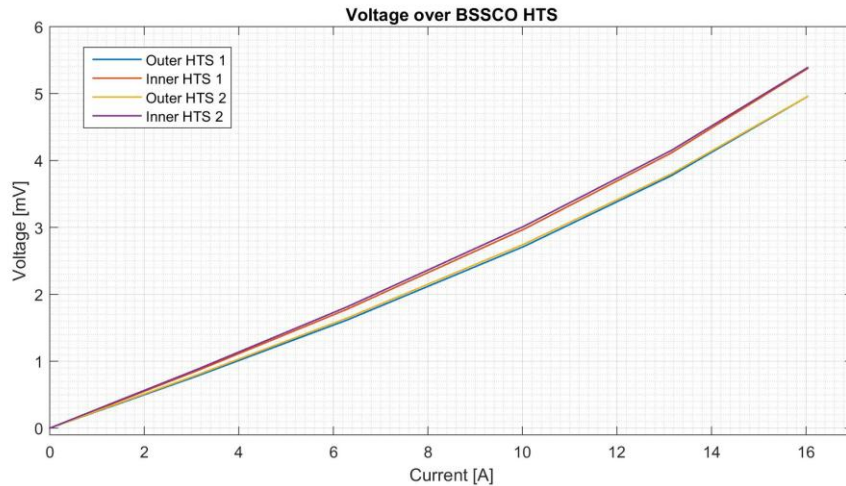


Figure 5.1: Voltage over the HTS current leads.

The 16 A current available in the initial testing was used to check the quality of the soldered joints, the turn-to-turn insulation and an initial check of the double pancake coils. Figure 5.2 shows the voltage drop over the nine joints between pancake coils. Joint 2 is the soldered joint between pancake coil 1 and 2. Joint 8 (between pancake coils 7 and 8) has a resistance twice as high as the others. However, the resistance is still only approximately 100 nΩ, an acceptable level at the well cooled position of the joints (100 nΩ yields a power dissipation of only 4 mW at 200 A and the combined power dissipation from the nine joints yield a power dissipation of 20 mW).

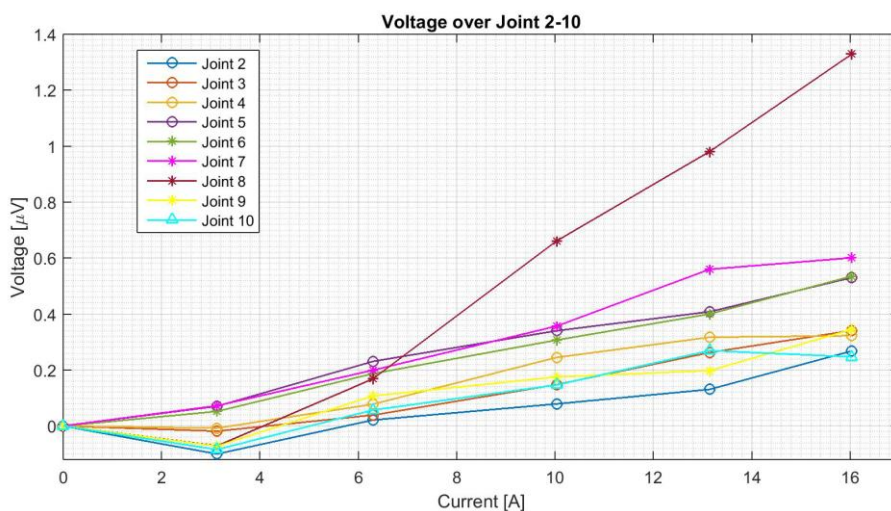


Figure 5.2: Voltage drop over soldered joints between pancake coils.

The voltage drop over the individual double pancake coils is shown in Figure 5.3. Seven coils show no voltage up to 16 A. The end coils, 1 and 10, and coil No. 6 show unwanted voltage drops.

After these first initial testing, the coil was warmed-up to room temperature, and the cryostat was opened. A gap between the 1st stage of the cooling machine and the radiation shield was revealed. A quick fix of the problem was attempted and the cryostat was closed and the coil again cooled down. However, the problem remained, and a more rigorous fix is needed. A temperature of about 140 K was measured on the radiation shield compared to the 70 K designed for.

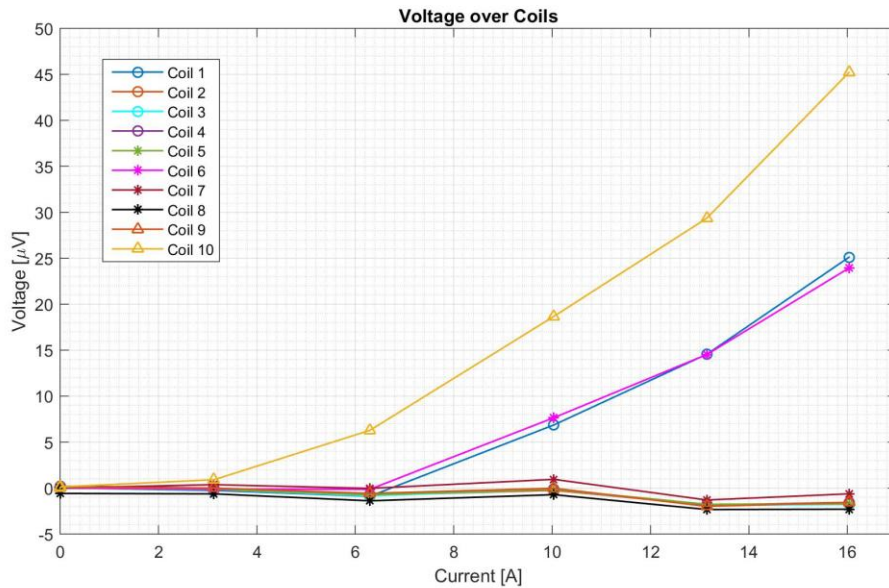


Figure 5.3: Voltage drop over the individual double pancake coils.

Figure 5.4 shows the voltage over and current in the coil during a slow ramping process. The results were used to calculate the inductance of the coil, $U = L \, di/dt$. The inductance, L , was calculated to 4.6 H, close to FEM-calculated values. Hence, there are no signs of turn-to-turn or layer-to-layer shorts within the coil.

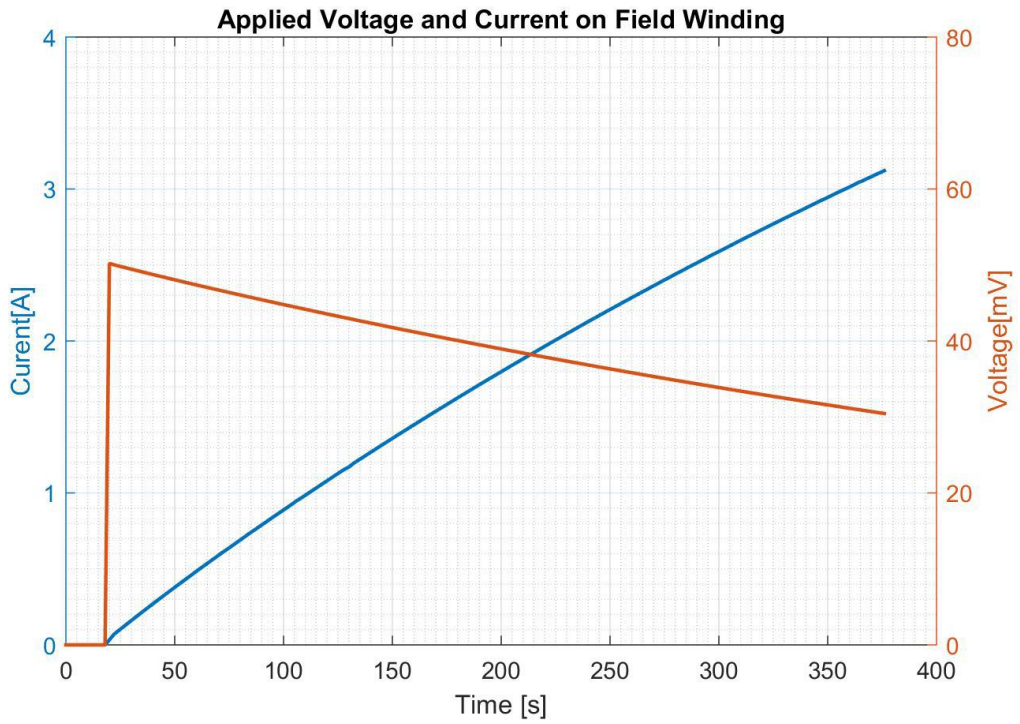


Figure 5.4: Current and voltage during a 6 minutes ramping sequence.

6 CONCLUSIONS

An MgB_2 superconducting generator pole has been designed, constructed and initially tested. The coil size corresponds to a full scale racetrack-shaped generator pole with the length of the straight section shortened to 0.5 m. In total 5 km of superconducting tape has been wet-wound with the epoxy between turns constituting the only electrical insulation.

Initial testing revealed problems with the current leads of the testing facility. Additionally, three out of the ten double pancake sub-coils showed unexpected voltage drops. It is unclear whether this voltage drop relates to a problem with the superconducting coils or the problems with the temperature in the testing facility. After solving the issue with temperature in the testing facility, proper testing can commence to determine the quality of the coil and test it at full load. A plan to accomplish such testing is outlined in chapter 7.

In spite of the problems mentioned above, the initial testing confirmed good soldered joints between pan-cake and good turn-to-turn electrical insulation (confirming the usability of the winding methodology).

7 ACTION PLAN TO COMPLETE A FULL LOAD TEST

The problem with the current leads encountered during initial testing is, in line with the observation after the first warm-up, probably related to insufficient cooling of the leads. This may be due to insufficient thermal anchoring of the current leads and radiation shield to the first cooling stage (40-80 K) of the cooling machine. Also, the voltages appearing over three coils may be related to the cooling issue. A too high temperature of the current leads could have transferred a too high temperature to the MgB_2 coil, particularly for coils No. 1 and 10. In case of an insufficient thermal anchoring of the first cooling stage, all three coils (and particularly the MgB_2 wires between the coil and the soldering position) could have resulted in a too high heat radiation leading to elevated temperatures in the MgB_2 wires explaining the voltages over coils No. 1, 6 and 10.

The following actions have been taken to solve the issue with a too high temperature of the radiation shield and current leads:

- Improved thermal anchoring of the current leads
- Improved thermal anchoring of the first cooling stage
- Placement of thermocouples on current leads, thermal shield, and first stage of cooling machine

These measures aim at allowing the full current to be passed into the coil. A cool down and measurement campaign should then reveal the status of the three coils initially showing voltage drops.

If the voltage drop remains in any coil, another warm up is planned and the coil(s) is short-circuited to allow for testing of the other coils at full load.

A third and a fourth cool-down are planned to be done during 2016. If a fifth cool down will be necessary, time is allocated in early 2017.

The results of these tests will be given in the final report of the workpackage.

References

- [1] Asger B. Abrahamsen, Niklas Magnusson, Bogi B. Jensen, Dong Liu and Henk Polinder, "Design of an MgB₂ race track coil for a wind generator pole demonstration", *Journal of Physics: Conference Series* vol. 507, 032001, 2014.
- [2] N. Magnusson, J.C. Eliassen, A.B. Abrahamsen, A. Nysveen, J. Bjerkli, M. Runde and P. King, "Design aspects on winding of an MgB₂ superconducting generator coil", *Energy Procedia* vol. 80, pp. 56-62, 2015.
- [3] Jan Christian Eliassen
Winding and Testing of Superconducting Coils
Master of Science Thesis, Norwegian University of Science and Technology, 2015.
- [4] Morten Ellingsen Paulsen
Assembly and Testing of Superconducting Field Winding
Master of Science Thesis, Norwegian University of Science and Technology, 2016.
- [5] Abrahamsen, A. B., Magnusson, N., Liu, D., Stehouwer, E., Hendriks, B., & Polinder, H., "Design study of a 10 MW MgB₂ superconductor direct drive wind turbine generator", In *Proceedings of EWEA 2014. European Wind Energy Association (EWEA)*.
- [6] Columbus Superconductors, Company web page, www.columbussuperconductors.com (visited Nov 2016).
- [7] Christian Bak, Frederik Zahle, Robert Bitsche, Taeseong Kim, Anders Yde, Lars C. Henriksen, Anand Natarajan, Morten Hansen, "Description of the DTU 10 MW Reference Wind Turbine", *DTU Wind Energy Report-I-0092* (2013).
- [8] INNWIND.EU deliverable D3.42 "First assessment of performance indicators of Superconducting direct drive and Pseudo magnetic direct drive generators" September 2013.
- [9] A.B. Abrahamsen, B.B. Jensen, E. Seiler, N. Mijatovic, V.M. Rodriguez-Zermeno, N.H. Andersen and J. Østergård, "Feasibility study of 5 MW superconducting wind turbine generator", *Physica C* 471 (2011) 1464–1469.
- [10] N. Magnusson, A.B. Abrahamsen, D. Liu, M. Runde and H. Polinder, "Hysteresis losses in MgB₂ superconductors exposed to combinations of low AC and high DC magnetic fields and transport currents", *Physica C* 506 (2014) 133–137.